

MODEL PATHWAYS IN LIGNIN THERMOLYSIS

by

Michael T. Klein (Doctoral Candidate)

and

Preetinder S. Virk (Associate Professor, Chemical Engineering)

ENERGY LABORATORY REPORT NO. MIT-EL 81-005

This report is a digest of a doctoral thesis submitted in February 1981 to the Department of Chemical Engineering, Massachusetts Institute of Technology, Cambridge, Mass.

The research was supported by seed funds from the MIT Energy Laboratory.

0748768

MODEL PATHWAYS IN LIGNIN THERMOLYSIS

by

Michael T. Klein and Preetinder S. Virk

Department of Chemical Engineering
Massachusetts Institute of Technology, Cambridge, MA 02139

TABLE OF CONTENTS

	Abstract.....	2
1.1	Introduction.....	3
1.2	Motivation.....	3
1.3	Lignin.....	4
1.4	Previous Pyrolyses.....	12
	1.4.1 Previous Lignin Pyrolyses.....	12
	1.4.2 Previous Model Compound Pyrolyses.....	19
	1.4.3 Limitations of Previous Work.....	22
1.5	Present Approach.....	23
	1.5.1 Analysis of Lignin Structure.....	23
	1.5.2 Selection of Model Compounds.....	27
	1.5.3 Simulation of Lignin Thermolysis.....	30
1.6	Experimental Methods.....	33
1.7	Experimental Results.....	37
	1.7.1 Phenethyl Phenyl Ether(PPE) Pyrolysis.....	37
	1.7.2 Summary of Experimental Results.....	55
1.8	Implications of Experimental Results.....	62
1.9	Simulated Lignin Thermolysis.....	66
1.10	Discussion.....	74
	1.10.1 The Mechanism of PPE Pyrolysis.....	74
	1.10.2 Comparison Between Simulated and Experimental Lignin Pyrolyses.....	80
1.11	Summary and Conclusions.....	90
1.12	References.....	93

MODEL PATHWAYS IN LIGNIN THERMOLYSIS

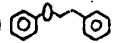
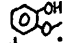
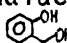
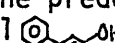
by

Michael T. Klein and Preetinder S. Virk

Department of Chemical Engineering
 Massachusetts Institute of Technology, Cambridge, MA 02139

ABSTRACT

A fundamental description of lignin thermolysis was attempted.

Analysis of the chemical topology of lignin suggested likely reaction pathways of import to lignin pyrolysis. In turn, 20 model compound pyrolysis substrates were selected to mimic the important reactive functional groups present in whole-lignin thermolysis. The more salient models were: phenethyl phenyl ether (PPE) , which depicts the most prevalent lignin interunit linkage, guaiacol , model of the predominant aromatic methoxyl, and saligenol  and cinnamyl alcohol , models of important propanoid side chains.

Detailed pathway and kinetic analyses and determination of reaction Arrhenius parameters provided mechanistic insights into the model compound pyrolyses. Several pericyclic reaction mechanisms, hitherto not mentioned in the lignin pyrolysis literature, were suggested. In particular, PPE likely pyrolyses via a concerted retro-ene mechanism, whereas guaiacol and saligenol may respectively eliminate methane and water by concerted group transfers.

A statistical interpretation of the lignin substrate coupled with the experimental model compound pyrolyses allowed simulation of whole-lignin thermolysis. The simulations were in substantial agreement with experimental pyrolyses reported in the literature in regard to overall gas, methane, carbon monoxide, individual phenols, and carbonaceous residue yields. Weight loss kinetics deduced from the time dependency of the latter yield also accorded well with the experimental literature.

1. Summary

1.1 Introduction

This thesis attempts a fundamental description of lignin thermolysis. A series of 20 different lignin model compounds were pyrolysed in the experimental portion of this work. A mathematical lignin thermolysis model was developed, based on both the experimental model pathways and a theoretical interpretation of lignin structure.

The investigation comprised three major components. First a critical examination of lignin and lignin chemistry was undertaken, aimed at discerning likely thermolysis reaction pathways. On the basis of this theoretical analysis, model compounds mimicking the essential reactive units of the whole-lignin substrate were selected and pyrolysed. The reaction pathways suggested by the model compound pyrolyses were then coupled with the structural analysis of whole-lignin to formulate a mathematical simulation model for whole-lignin thermolysis. Hence, the experimental model compound results were coupled with the theoretical analysis in an effort to describe the essential features of whole-lignin thermolysis.

1.2 Motivation

The increased utilization of biomass and coal resource bases must be accompanied by an enhanced understanding of the fundamental events effecting their thermal processing. The elucidation of these fundamentals should greatly assist in the selection of catalysts, solvents, and process operating conditions for optimal substrate conversion, as well as provide insight into the expected results of operating in regions devoid of experimental details. The objective of this investigation is an elucidation of the important reaction pathways and mechanisms involved in lignin pyrolysis, with an aim toward providing a rationalization and prediction

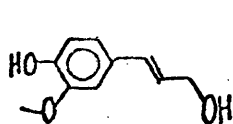
of observed lignin pyrolysis products and kinetics.

Lignin is a major component of biomass, accounting for up to about 36% of wood by weight. The U. S. coal reserve is composed of predominantly lignite, subbituminous, and bituminous coals, the respective percentages being 28%, 27%, and 43%.² In view of the evolutionary linkage of lignin to low rank coal, the high percentage of low rank bituminous and lignitic coals suggests that lignin thermolysis may be relevant to many aspects of coal pyrolysis.

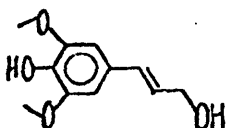
Both coal and lignin are ill-defined refractory substrates which lack unequivocal chemical structures. Their pyrolyses yield complex and poorly characterized product spectra. Thus, the reaction pathways and mechanisms involved in the pyrolyses of these complex substrates have remained obscure. This motivated the use of model compounds, where the products from pyrolysis of a well defined substrate may be used to infer reaction pathways, kinetics, and mechanisms.

1.3 Lignin

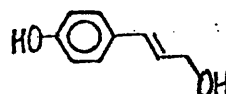
Pure lignin is a natural phenolic polymer composed of carbon, hydrogen, and oxygen. The ultimate lignin precursors are carbon dioxide and water, biosynthetic fixation of which⁴ produces coumaryl, coniferyl, and sinapyl alcohols, shown below. These three alcohols are the sole



CONIFERYL



SINAPYL



COUMARYL

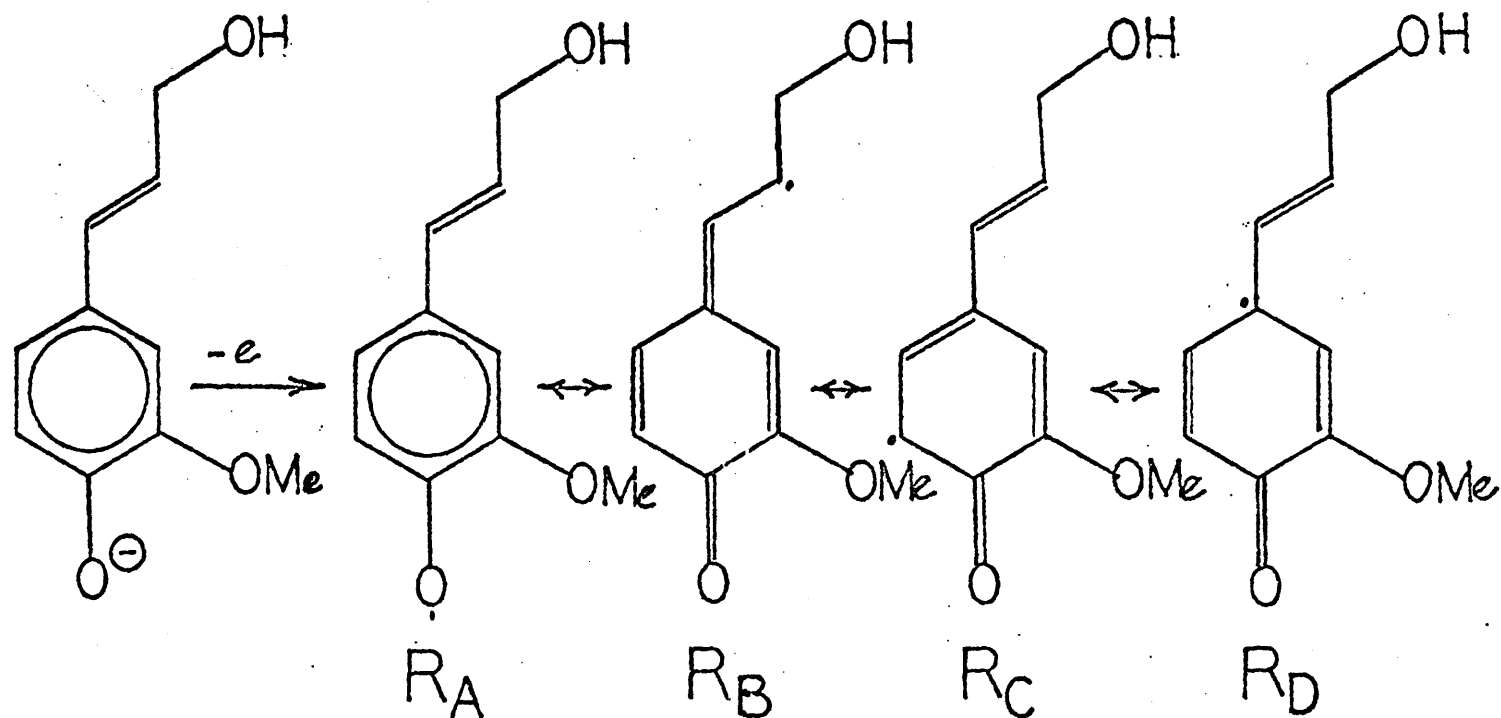
monomeric precursors to lignin, with coniferyl alcohol predominant.

Natural lignification can be artificially duplicated by the enzymatic, oxidative dehydrogenation of coniferyl alcohol, which eventually yields an amorphous polymer very similar to conifer lignin. The mechanisms

and pathways of lignin growth have been ascertained by the isolation of intermediates, termed lignols, of this process. According to Freudenberg⁴, the classic reference on the subject, lignification proceeds thus.

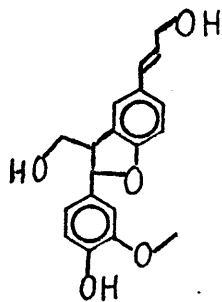
Under the action of enzymes like laccase, the phenolate anion of coniferyl alcohol is converted to a phenoxy radical. This radical enjoys a half life of about 45 seconds⁵, being stabilized by resonance as depicted in Figure 3.3. The major lignification growth mechanism is the coupling of these free-radical species, the most important coupling mode being the combination of an R_a and R_b radical. This is shown in Figure 3.4. The resulting quinonmethide (IV) will generally add water in a nucleophilic manner to yield the guaiacyl-glycerol- β -coniferyl ether (V). This β -ether is the most prevalent link in the lignin macromolecule. However, the nucleophilic component of this reaction can be varied considerably. For example, guaiacyl-glycerol- α,β -diconiferyl diether (VI) represents the addition of coniferyl alcohol to the quinonemethide. Plant sugars and polysaccharides also compete for addition to the quinonemethide, representing the main pathway for formation of lignin-carbohydrate covalent bonds. Similar coupling reactions of each radical form R_a - R_d , as well as coupling of the higher lignols, accounts for the molecular weight increase attending lignification.

Of direct importance to this investigation is a representation of the types and proportions of the moieties and bonds which constitute lignin. This information is conveyed in the classic schematic structural representation of Freudenberg⁴, shown in Figure 3.5. This formula is not to be interpreted as a literal, unequivocal chemical structure for lignin, but rather as a schematic depiction of the structural insights gleaned from experiment. Harkin⁵ draws an analogy between lignin and playing cards,

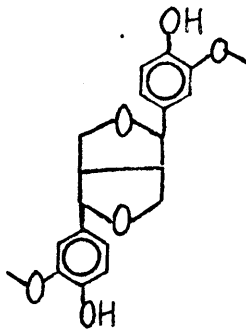


CONIFERYL ALCOHOL RADICAL

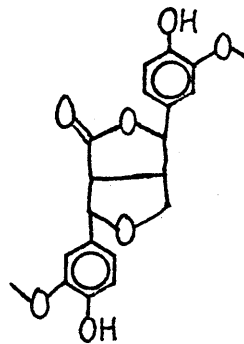
Figure 3.3 Resonance forms of coniferyl alcohol radical.



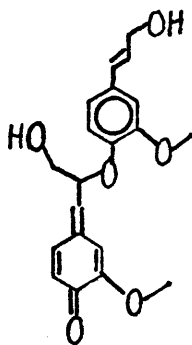
I



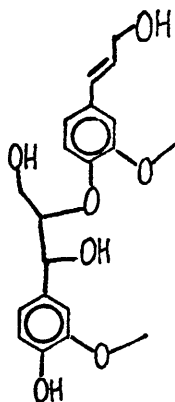
II



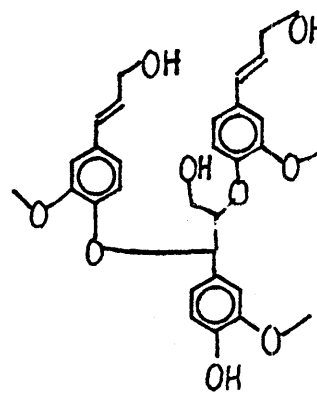
III



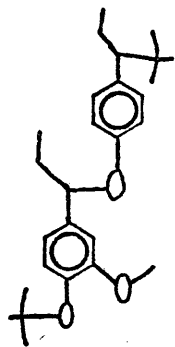
IV



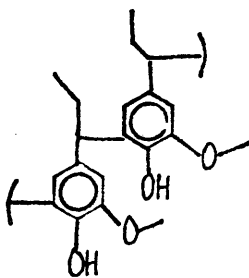
V



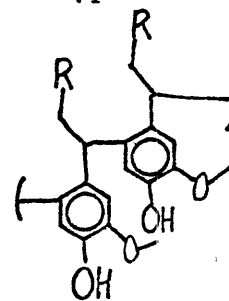
VI



VII



VIII



IX

Figure 3.4 Typical lignification lignols.

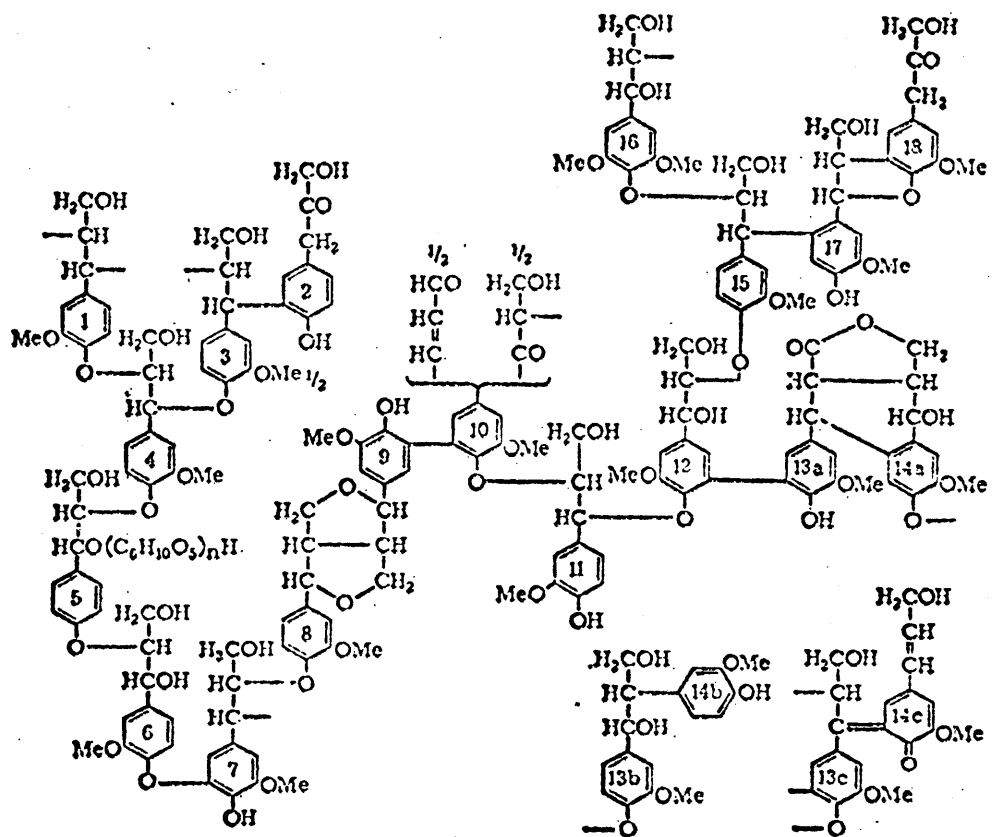


Figure 3.5 Freudenberg lignin structural model.⁴

emphasizing the existence of a broad statistical distribution of well known but also well shuffled chemical structures that cannot possibly be represented in one formula. Only in the limit of infinite statistical sampling, or infinite schematic formula size can lignin structure truly be realized. This emphasizes the importance of bond and moiety types and their frequency distributions in lignin description. Note, for example, that the linkages between units 1-4, 4-5, 5-6, 7-8, 10-11, 12-15, and 15-16 in Figure 3.5 are all of the β -ether type. This is clearly the single most predominant interunit linkage.

For the present purposes the best characterization of Freudenberg's structure was effected in terms of the phenolic units and the propanoid side chains of each monomer. Figure 3.7 schematically represents the types of methoxyphenol units in Figure 3.5. The three monomer alcohols are divided into two types, those with etherified hydroxyls and those with free phenolic hydroxyls. The former category is further subdivided according to ether type. Because of the large percentage of coniferyl alcohol monomer incorporated into the lignin macromolecule, guaiacols, either free or β -etherified, account for the largest proportion of the methoxyphenol units in a spruce lignin. The propanoid side chains occurring in Figure 3.5 are shown in Figure 3.8. Despite the apparent complexity of the Freudenberg structure, there exist but eight side chain types. The most prevalent of these is the β -etherified guaiacyl-glycerol moiety, which occurs, e.g., as the side chain to unit 6. The mechanisms of lignification suggest that while the side chain of one aromatic unit may be involved in a lignin linkage with the guaiacyl moiety of another monomeric unit, it cannot be involved in bonding with its own guaiacyl moiety. With regard to the Freudenberg structure, this point implies that the side chain shown for

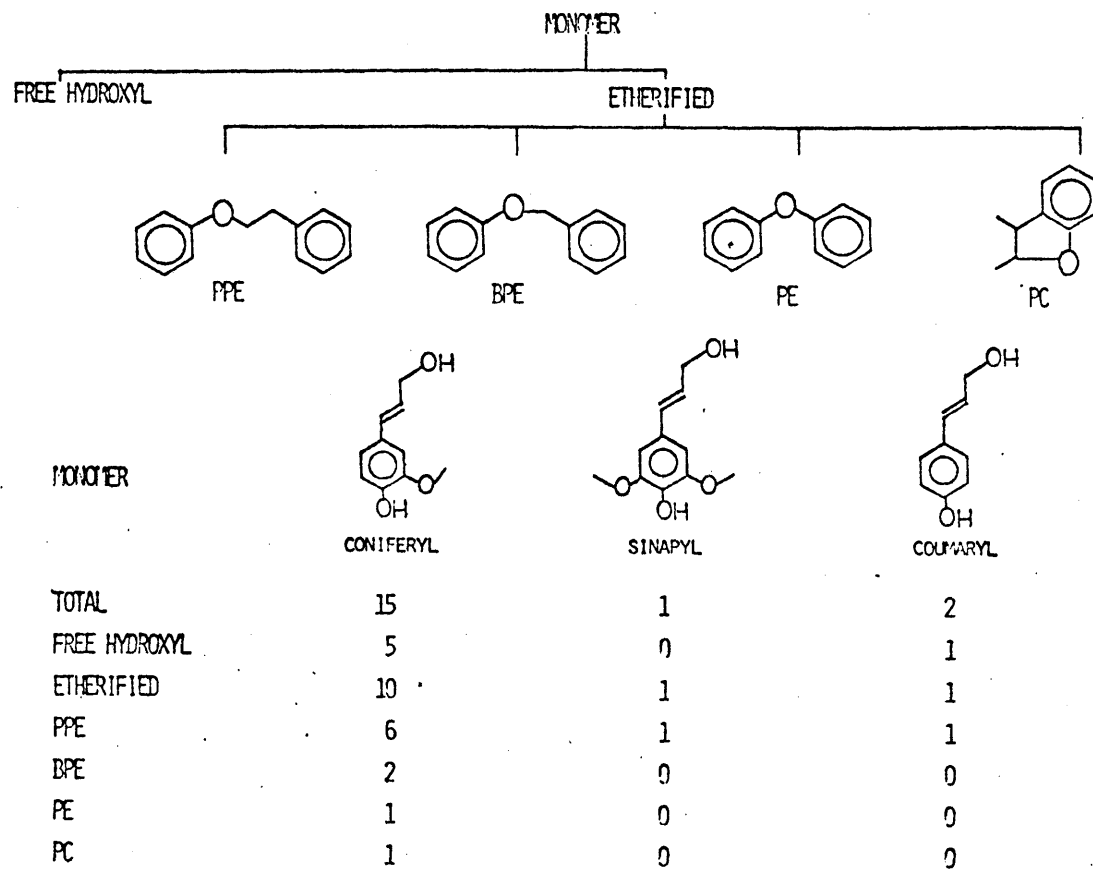


Figure 3.7 Distribution of lignin methoxyphenols as found in the Freudenberg model.

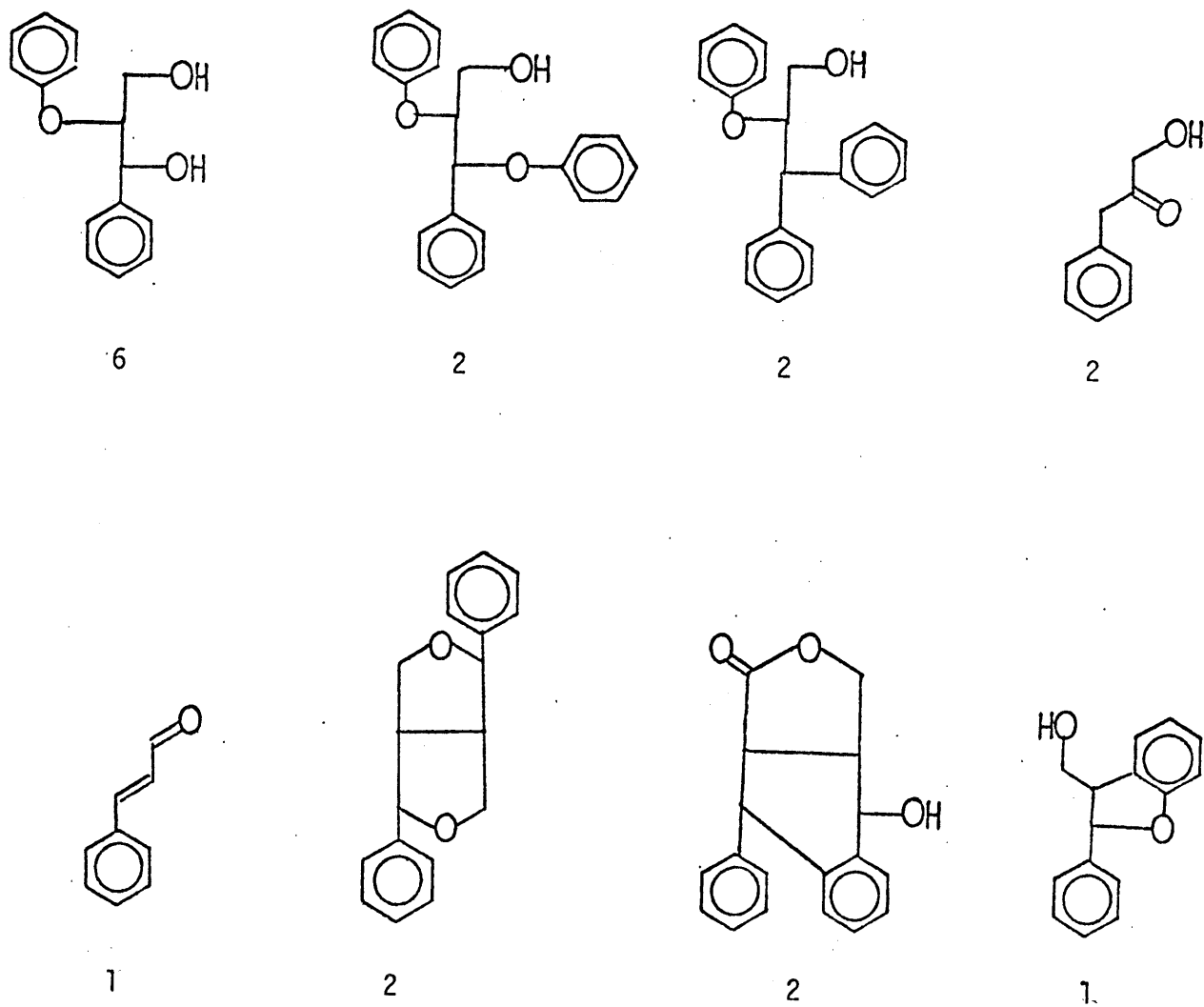


Figure 3.8 Distribution of 3-carbon side chains as found in the Freudenberg model.

unit 6, for example, might be associated with any of the methoxyphenol moieties shown for units 6, 7, 8, and 3, in proportions related to the probabilities of the given methoxyphenol and side chain unit derived from Figures 3.7 and 3.8.

1.4 Previous Work

A major goal of the present work was elucidation of the fundamental reaction pathways involved in lignin pyrolysis. This section will consider previous pyrolyses of lignin and lignin model compounds.

1.4.1 Previous Lignin Pyrolyses

Figure 4.1 is a summary of major lignin pyrolysis products and Table 4.1 is a representative listing of the major pyrolysis products reported in the literature.

Gases
As illustrated in Table 4.1, total gas yields average 15% by weight of lignin pyrolysed, the major product gases being CH_4 , CO , CO_2 , and ethane. Heuser and Skioldebrand²³ obtained a gas consisting of 50.9% CO , 37.5% CH_4 , 9.6% CO_2 , and 2% ethane from pyrolysis of an HCl spruce lignin, while Gladkova, et al.²⁵, reported 25% CO , 48% CH_4 , and 11% CO_2 in the product gas from pyrolysis of a hydrolysis hardwood lignin. In both cases the high contents of CO and CH_4 , and the rather low content of CO_2 , are noteworthy. Iatridis and Gavalas²⁶ pyrolysed a Douglas fir Kraft lignin; the major gaseous products were CH_4 , CO , and CO_2 , with minor amounts of other hydrocarbon gases also. The ratio CO/CH_4 exhibited an interesting variation with temperature. At 400 C, CO/CH_4 was approximately 2.3 while at 500 C this ratio dropped to roughly 0.85, and finally at 550 through 650 C the ratio climbed to values approaching 2. The relatively large CO_2 content, typically 6%, observed by these authors is inconsistent with previous literature citations, and likely arose from modification of

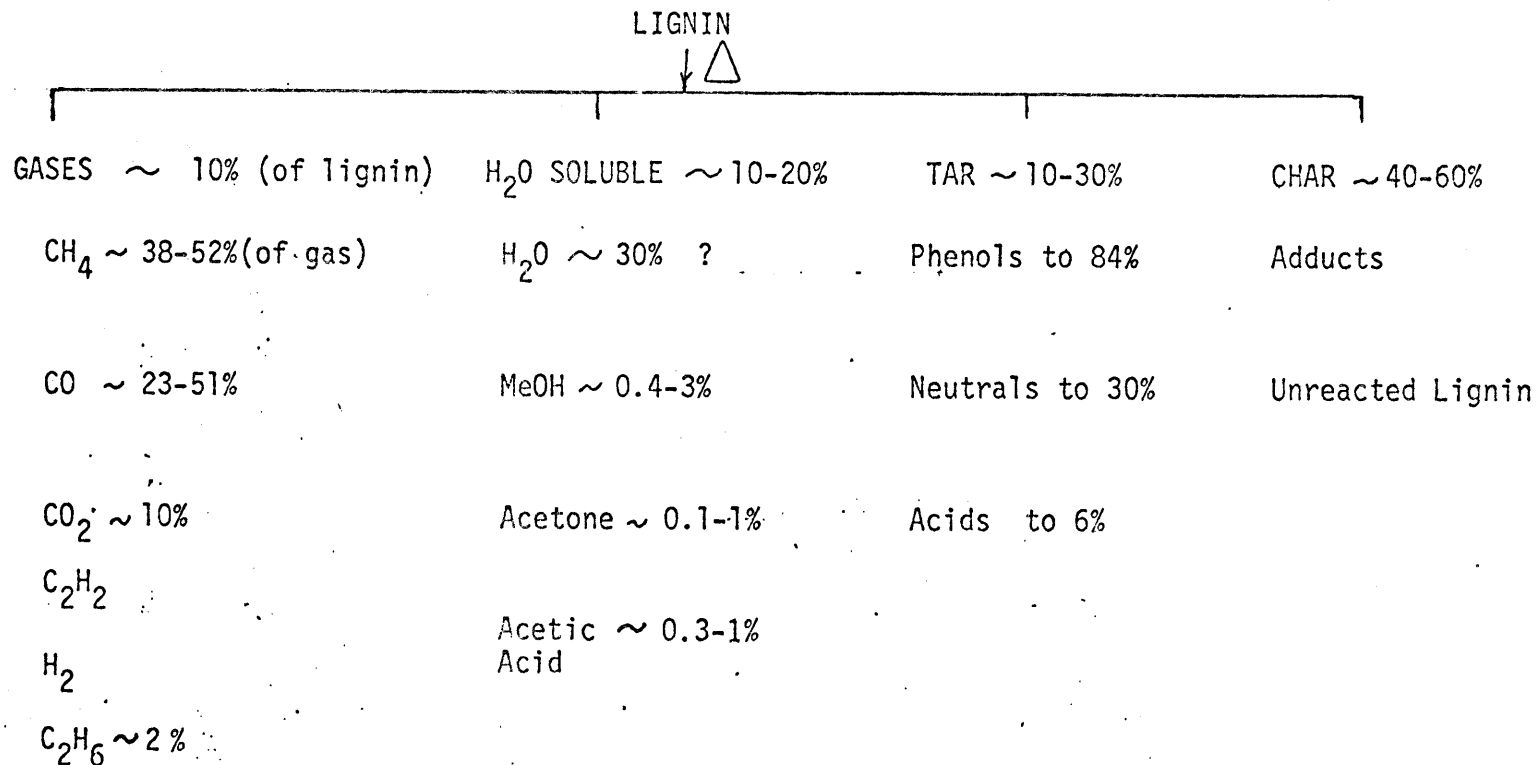


Figure 4.1 Schematic of overall lignin pyrolysis product spectrum

Reference	Material Pyrolysed	Char		Tar		Aqueous		MeOH		Acetone		Ac. Acid		Gas		CO		CH ₄		CO ₂		Other	
		←	→	←	→	←	→	←	→	←	→	←	→	←	→	←	→	←	→	←	→	←	→
(52) 1975	Lignin	63.5	7.2	16.4											12.9								
(35) 1938	Alk. corn stk. Lig	57	19.5	11.8				.28	.28	.43					11.7								
(34) 1929	Alk. Lig	52.2	17.7	15.5				1.9	.13	.05					13.5								
	HCL Lig	58.5	7.5	15.1				.7	.57	1.1					19.1								
	H ₂ SO ₄ Lig	65.5	7.4	15.0				1.1	1.0	.9					11.5								
(31) 1928	Oak Lig	50-6	3					1.5	.21	1.3													
	Birch Lig	50-6	4					1.4	.18	1.3													
	Beech Lig	50-6	5					1.0	.22	1.3													
(23) 1919	Spruce Lig	50.6	13					.9	.19	1.1					50.9	37.5	9.6				C ₂ H ₆	2.	
(53) 1918	Aspen Lig	45.0	9.6					.7	.10	.64													
(24) 1907	Cellulose	34.9	6.3					0.0	.13	2.8					32.4	3.12	62.9				C ₂ H ₆	1.6	
	Wood	37.8	8.1					.96	.20	3.2					32.6	9.3	56.5				C ₂ H ₆	1.7	
(32) 1925	HCl Aspen	44.3	14.3					.87	.22	1.3													
(25) 1974	Hydr. Lig	40.5	14.2												23-7	44-52	10-2						
(29)															+	+	+					C ₂ H ₂	18
(27) 1975															+	+	+					H ₂	
(54) 1932	Alk. corn	50.5	28.3	11.7				.65	.1	.3					9.3								
(55) 1920	HCl Lig	57.2	12.5	13.2											17.0								
(56) 1921	HCl spruce	53.8	10.2	14.2																			
(57) 1923	HCl spruce	52.0	15	21																			
(58) 1952	HCl	60	7	20											15								
(59) 1955	H ₂ SO ₄	56		19											10-3								
(60)																							
	1950 HCl	44-8		35-7											17-8								
(61) 1958			30	8.7																			
(62) 1947		55.66	5-9	13-21				.4	.2	.3													
(52) 1970	400 C	63.5	7.2	16.4											12.9								
	500 C	54.7	7.4	20.4											17.4								
	600 C	51.0	7.6	22.1											20.4								
(63) 1970		42	21												20								
(26)	IATRIDIS AND GAVALAS DETAILED SEPARATELY																						

Table 4.1 Representative products from lignin pyrolysis.

their lignin during Kraft pulping.

Aqueous Distillate Products

Aqueous distillate yields from pyrolysis amount to roughly 20% by weight of the lignin charged. Its main constituents are water, methanol, acetic acid and acetone.

Methanol is formed in yields ranging from 0.3% to 3% of the lignin; this corresponds to about 10% of the lignin methoxyl content.¹⁹ Klason²⁴ pyrolysed wood from birch, beech, pine and spruce and found the yield of methanol from the former two hardwoods twice as high as that from the latter two softwoods. Other observations^{23,31} also show that hardwood lignins yield more methanol than softwood lignins. Because hardwood lignins incorporate a larger proportion of dimethoxylated sinapyl alcohol monomer units than do softwoods, Allan and Matilla³⁰ have suggested that methanol originates from methoxyl moieties in lignin.

The acetic acid and acetone produced from lignin pyrolysis presumably originate in the three carbon phenylpropane unit. Allan and Matilla³⁰ report that the yields of acetic acid from hardwoods are significantly higher than those from softwoods. This is attributed to the hardwoods possessing a less condensed lignin polymer than the softwoods. In general, as seen in Table 4.1, acetone yields are considerably lower than those of acetic acid and methanol. The data of Iatridis and Gavalas²⁶ show significant yields of methanol and acetone, but do not include acetic acid.

Water is the major component of the aqueous distillate fraction; water yields of 10%-20% of the lignin are typical, as shown in Table 4.1. Extensive hydrogen bonding between hydroxyl groups and other oxygen moieties in lignin is likely responsible for the rather facile loss of

water during pyrolysis. However, the mechanistic aspects of water release are poorly understood. Also, interpretation of water yield data is complicated by the inevitable presence of physically bound water in lignin samples.

Tars and Oils

The tar fraction resulting from lignin pyrolysis has received considerable attention due to the high proportion of valuable phenols in it. As seen in Table 4.1, the tar yield is typically 15%-20% by weight of the lignin. The lignin isolation method exerts a significant influence on tar yields^{34,39}. Thus pyrolysis of alkali, HCl, and H₂SO₄ lignins³⁴ yielded 17.7%, 7.5%, and 7.4% tar yields, respectively. In the rapid thermolysis of alkali, HCl, and H₂SO₄ lignins³⁹, the alkali lignin yielded the largest proportion of phenols; it was also noteworthy that lignins from different woods isolated by the same method were much more similar than lignins from the same wood isolated by different methods.

Table 4.5 is a representative listing of phenols identified in the tar product. The phenols detected mirror the constituent lignin monomers. Thus, guaiacol and catechol derivatives predominate, with sinapyl and coumaryl units in evidence as well. The singly oxygenated phenols likely arise from reactions of the guaiacyl and sinapyl moieties and also from degradation of coumaryl alcohol monomers. Phenol substitution is invariably in the para position, and often includes all three carbons of the original propanoid side chain.

The Carbonaceous Residue

A carbonaceous residue is a prevalent lignin pyrolysis product. Chemical analysis of this product has rarely been effected, though Gillet and Urlings⁴⁸ found that coke from a Brauns and from an ethanolysis lignin

Table 4.5 Phenols Reported From Lignin Thermolysis

PHENOL	REFERENCE
1 Phenol	43,35,39,58,62,54, 42,41, 26
2 o-cresol	{43,40,35,39,42,58,62, 26,54,41
3 m,p-cresol	
4 m-ethylphenol	40
5 p-ethylphenol	43,49, 40
6 p-propylphenol	40
7 xylenols	40,35,58,62, 42,41
8 guaiacol	43,40,35, 41,39,58,62, 34,44, 42,26
9 p-methylguaiacol	35,39, 58,41,62, 44, 42,26
10 p-ethylguaiacol	30,58,62,44,26,41,42
11 p-propylguaiacol	39,54,41,42
12 eugenol	39,32,41
13 isoeugenol	39,41
14 vinylguaiacol	39,54,38,41
15 coniferaldehyde	38
16 vanillin	38,41,42
17 acetovanillone	39,42
18 propiovanillone	41
19 vanillic acid	41
20 catechol	39,38,65,41,54
21 p-methylcatechol	39,38,41
22 p-ethylcatechol	39
23 syringol (DMP)	39, 42,44, 41
24 p-methylsyringol	39,44, 41,42
25 p-ethylsyringol	42
26 p-propylsyringol	38,41,42
27 vinylsyringol	39,41
28 allylsyringol	39
29 syringaldehyde	38
30 acetosyringone	41
31 propiosyringone	41
32 methoxycatechol	38,41

SEE ACCOMPANYING ILLUSTRATION FOR CHEMICAL STRUCTURES

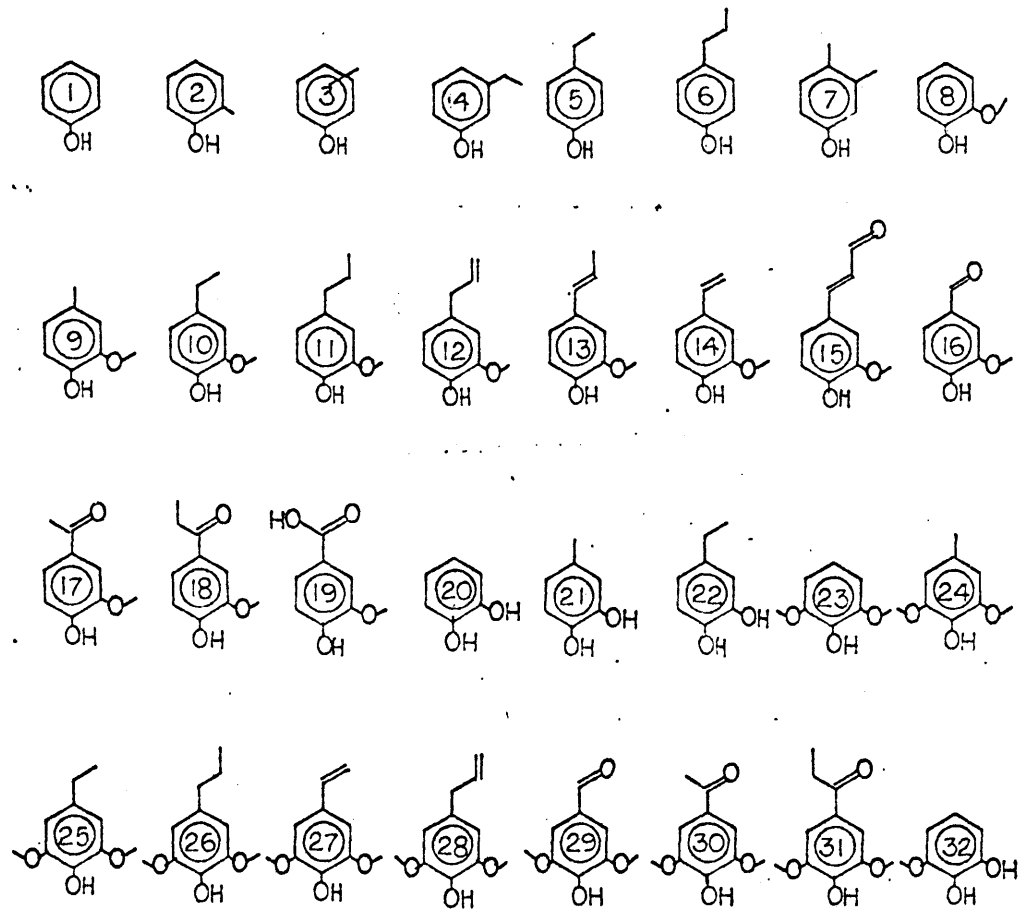


Table 4.5 (cont.) Chemical Formula key

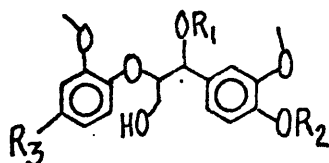
each had an elemental composition similar to that of a Rhenish lignite. Their elemental formula of $(C_{40}H_{30}O_{11})_2$ is represented in Figure 4.2 by their speculative coke structure.

1.4.2 Previous Model Compound Pyrolyses

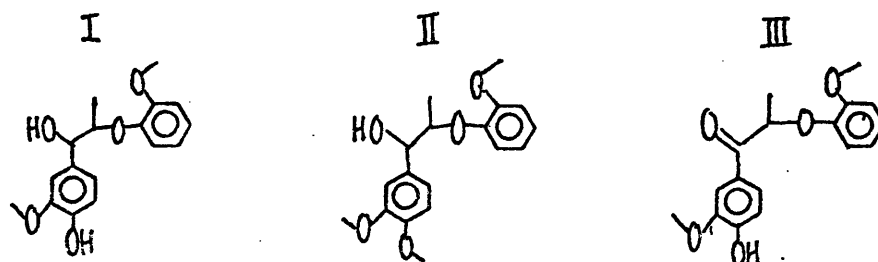
Previous model compound studies may be organized into three groups: the lignin interunit linkages, the methoxyphenols, and the 3-carbon side chain units.

Lignin Interunit Linkages

The most prevalent lignin interunit linkage is the β -ether linkage, which can be represented, in the lignin, as:



The thermal behavior of these β -ether linkages has been studied by two investigators^{75,76}. Domburg⁷⁵ studied the substituted β -ethers I, II, and III. The temperature for 50% weight loss for each of these were reported, from Differential Thermal Analysis (DTA) experiments conducted at 12C/min, as



I(280 C)<II(310 C)<III(365 C). Activation energies of 16, 15, and 82 kcal/mol were also reported for I, II, and III respectively. The product spectra consisted of guaiacol, methyl-, ethyl-, and propyl-guaiacols, cis- and trans-isoeugenol, vanillin and acetovanillone, the latter two forming in much larger quantities from III than either I or II. The large predominance of guaiacol products appears indicative of a formal scission of the β -carbon

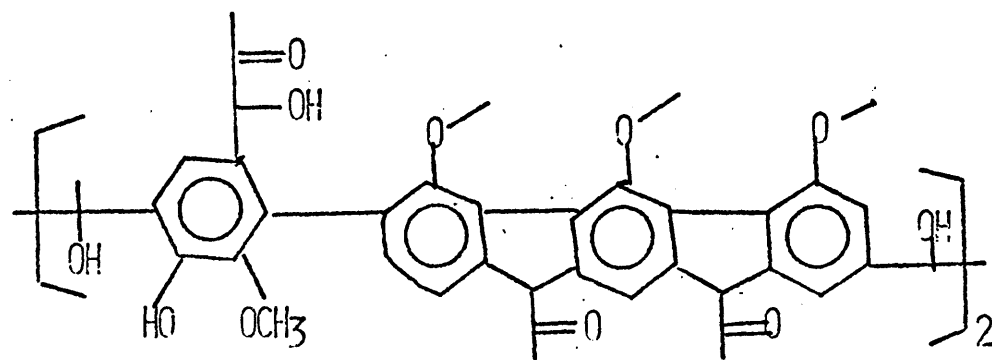
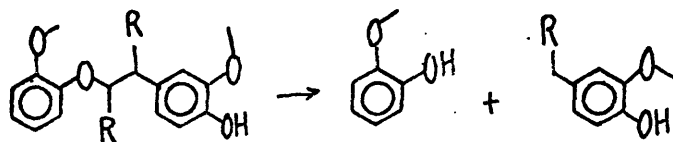
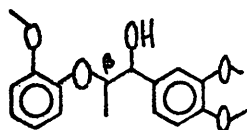


Figure 4.2 Schematic coke structure of Gillet & Urlings⁴⁸

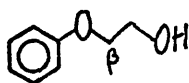
oxygen linkage:



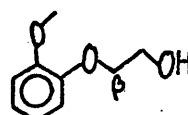
Savinykh⁷⁶ probed the effect of methoxyl and phenyl substituents on the thermal behavior of lignin β -ethers. They heated compounds II, IV and V to 500 C at a rate of 5C/min. The temperatures for 10% weight loss were



II



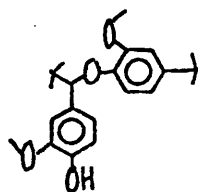
IV



V

II(300C)<<V(380C)<IV(400C). The most pronounced effect is that of veratryl substitution(cf V,II); compound II also differs from V in methyl substitution at the β carbon of II, but this is likely a minor factor in comparison with the veratryl substituent.

Another prevalent link in the lignin macromolecule is the α aryl ether bond, as in:



The decomposition of α -aryl alkyl ether bonds, as in benzyl phenyl ether (BPE), appears to be a rather facile process for the conditions of interest here^{79,80,81}. A conversion of 31% at 320 C and 30 minutes holding time was reported⁷⁹, with phenol, toluene, and benzylphenol as predominant products.

Methoxyphenols

The aromatic methoxyl unit is a characteristic moiety of lignin. Pyrolyses of several related model compounds have been reported, including

guaiacol^{91,92,93,94} and veratrole,^{91,92} which model free hydroxylic and etherified methoxyphenols, respectively. Pyrolyses have also been reported for anisole^{91,95,96,97,82} and 2,6-dimethoxyphenol(DMP)⁹¹. In these previous pyrolyses of veratrole, anisole and guaiacol, demethylation, demethoxylation, and isomerization reactions have been found to occur. In the temperature range 400-600 C, demethylation seems modestly predominant for guaiacol and veratrole, but overwhelmingly predominant for anisole. However, the literature pyrolyses have been effected at rather high conversions, which permit significant secondary reactions and thus provide product spectra little indicative of reaction pathways.

Side Chain Units

Previous experiments relating to lignin side chain unit pyrolyses arise both from lignin-related and other experiments. In general, hydroxylic side chain units appear to undergo dehydration^{99,100,101} and isomerization reactions¹⁰⁰, with reactivity dependent upon the structure of the side chain and substituent groups. Carbonyl side chains are reported to undergo decarbonylation with evolution of CO; e.g., benzaldehyde yields CO and benzene at temperatures of 400-500C, by a mechanism quite likely molecular in nature.^{98,82}

1.4.3 Limitation of previous work

Previous lignin pyrolyses provide little fundamental insight into the mechanisms and pathways of degradation. This is due, in part, to the wide range of lignin types, lignin isolation methods, and lignin pyrolysis reactors employed. Further, the complex product spectra obtained have thus far defied efforts to unequivocally elucidate the origins of individual products.

Previous model compound pyrolyses provide some insight into possible

lignin pyrolysis reactions, but fail to detail either product spectra or primary reaction pathways. Few kinetic parameters are reported. Further, many studies employ non-isothermal DTA and DTG techniques, the latter being particularly difficult to interpret since chemical transformations, e.g. isomerizations, need not be attended by weight loss. Finally, it is significant that previous model compound studies have never hitherto been applied to describe whole-lignin pyrolysis.

1.5 Present Approach

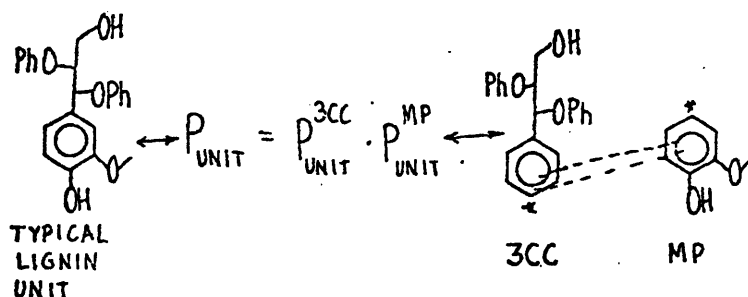
The present approach involved analysis of the lignin to suggest formal reaction pathways for lignin thermolysis. This permitted development of a list of model compounds to be experimentally pyrolysed. Pyrolysis results, combined with the earlier lignin structural analysis, then allowed a mathematical simulation of whole-lignin thermolysis in a manner comparable with available experiments.

1.5.1 Analysis of Lignin Structure

Lignin is a random co-polymer of coniferyl, sinapyl and coumaryl alcohol monomers. The single ring aromatic units in lignin possess, at positions 1, 3, and 4, respectively, a 3-carbon chain, methoxy, and phenol substituents. These aromatic units are connected by interunit linkages of (in descending prevalence) β -ether, α -ether, diphenylmethane, diarylether, diaryl, pinoresinol, and phenylcoumaran types. Thus lignin is simply an ensemble of single ring aromatic units, linked by seven types of interunit bonds.

An essential feature of lignin constitution, noted earlier, is that while the methoxyphenol of a given aromatic unit may be involved in bonding with the 3-carbon chain or methoxyphenol of an adjacent unit, it is never involved in bonding with the 3-carbon chain of the same aromatic

unit. Thus the nature of methoxyphenol substitution on a given aromatic unit is independent of the nature of 3-carbon side chain substitution on the same unit. Thus, as illustrated below, the probability of the occurrence in lignin of a given aromatic unit must be equal to the prob-



ability of the proper side chain multiplied by the probability of the proper methoxyphenol. This is the probability of the simultaneous occurrence of two independent events, namely the product of the individual probabilities, i.e., P_A and $B = P_A \times P_B$.

The present probabilistic interpretation of the Freudenberg lignin structure can now be elaborated. Figure 5.1 is a numerical summary of the types of aromatic units present in the Freudenberg structure of Figure 3.5. The grid points in Figure 5.1 show the 18 aromatic unit types depicted in the Freudenberg structure, and are positioned in the grid so as to represent the appropriate match of methoxyphenol and 3-carbon side chain substituents. The present interpretation of the Freudenberg structure is schematized in Figure 5.2. Using the distributions of 3-carbon side chains and methoxyphenols detailed in Figures 3.7 and 3.8, a grid of 18 total aromatic units has been generated by multiplying all possible methoxyphenol types against all possible 3-carbon side chain substituent types. Thus, many of the grid points with zero entries in Figure 5.1 now have non-zero entries in Figure 5.2;

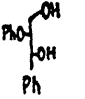
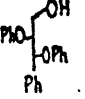
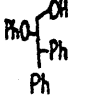
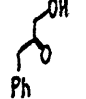
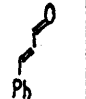

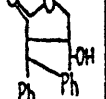
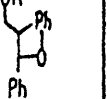
MP \ 3CC									Σ MP	
CONFERYL ALCOHOL	FREE	1	1	0	0	-0	1	1	1	5
	ETHER	3	1	2	1	1	1	1	0	10
COUMARYL ALCOHOL	FREE	0	0	0	1	0	0	0	0	1
	ETHER	1	0	0	0	0	0	0	0	1
SINAPYL ALCOHOL	FREE	0	0	0	0	0	0	0	0	0
	ETHER	1	0	0	0	0	0	0	0	1
Σ 3CC		6	2	2	2	1	2	2	1	18

Figure 5.1 Aromatic unit grid : Freudenberg structure

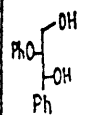
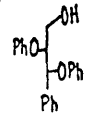
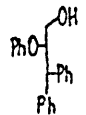
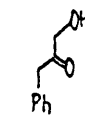
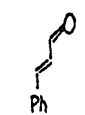

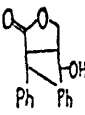
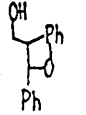
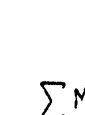
MP \ 3CC										\sum MP
NORMALIZED DISTRIBUTION	(.33)	(.11)	(.11)	(.11)	(.06)	(.11)	(.11)	(.06)	(1)	
CONFERYL ALCOHOL										
FREE (.28)	1.66	.55	.55	.55	.30	.55	.55	.30	5	
ETHERIFIED (.56)	3.33	1.11	1.11	1.11	.60	1.11	1.11	.60	10	
COUNARYL ALCOHOL										
FREE (.055)	.327	.11	.11	.11	.060	.11	.11	.060	1	
ETHERIFIED (.055)	.327	.11	.11	.11	.060	.11	.11	.060	1	
SINAPYL ALCOHOL										
FREE (0)	0	0	0	0	0	0	0	0	0	
ETHERIFIED (.055)	.327	.11	.11	.11	.060	.11	.11	.060	1	
\sum 3CC (1)	6	2	2	2	1	2	2	1	1	

Figure 5.2 Aromatic unit grid : Present approach

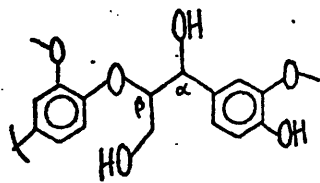
correspondingly, the proportions of certain overemphasized aromatic units in Figure 5.1 have been reduced.

This investigation will use the preceding statistical matching approach to describe whole lignin.

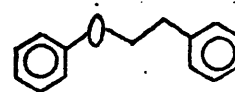
1.5.2 Formal Pathways in Lignin Thermolysis: Selection of Model Compounds

At the temperatures of interest in most lignin thermolyses, the aromatic units will persist. Thus, the essential reactivity of whole-lignin will be that of the methoxyphenols, 3-carbon side chains, and interunit linkages. Consideration of such units present in the Freudenberg structure generated a set of compounds capable of describing the essential features of lignin pyrolysis. Table 5.1 lists these model compounds. A complete discussion of the logic used to arrive at this list is presented on the main text of this thesis.

The prevalent guaiacyl β -ether link, structure I, was modelled as phenethyl phenyl ether (PPE), compound 1. PPE contains the essential β -ether carbon-oxygen link but does not possess the α -hydroxy, β -methylol and guaiacyl substituents present in the actual lignin moiety. The effects of these substituents (which can be accounted for theoretically and experimentally) should be of second order importance^{75,76} as compared to the basic reactivity of the β -ether link.



(I)



(1) phenylethyl-phenylether, PPE.

Of particular significance are the reactions of the β -ether. Formal reversion of the guaiacyl-glycerol- β -ether may generate a guaiacol type

Table 5.1 Model Compounds to be Pyrolysed

Interunit linkages

1.	Phenethylphenylether	PPE
2.	o-hydroxydiphenylmethane	OHD
3.	phenylether	PE
4.	biphenol	BPhOH
5.	biphenyl	BP

Methoxy phenols

6.	guaiacol	G
7.	veratrole	VE
8.	anisole	AN
9.	2,6-dimethoxyphenol	DMP
10.	isoeugenol	I
11.	vanillin	VA

Carbonyl Units

11.	vanillin	VA
12.	benzaldehyde	BA
13.	acetophenone	AP
14.	cinnamaldehyde	CAD

Propanoid side chains

14.	cinnamaldehyde	CAD
15.	cinnamylalcohol	CAL
16.	saligenol	SAL

CO₂ precursors

17.	ferulic acid	FA
18.	cinnamic acid	CA
19.	1-napthoic acid	1NA
20.	2-napthoic acid	2NA

SEE ACCOMPANYING ILLUSTRATION FOR CHEMICAL STRUCTURES

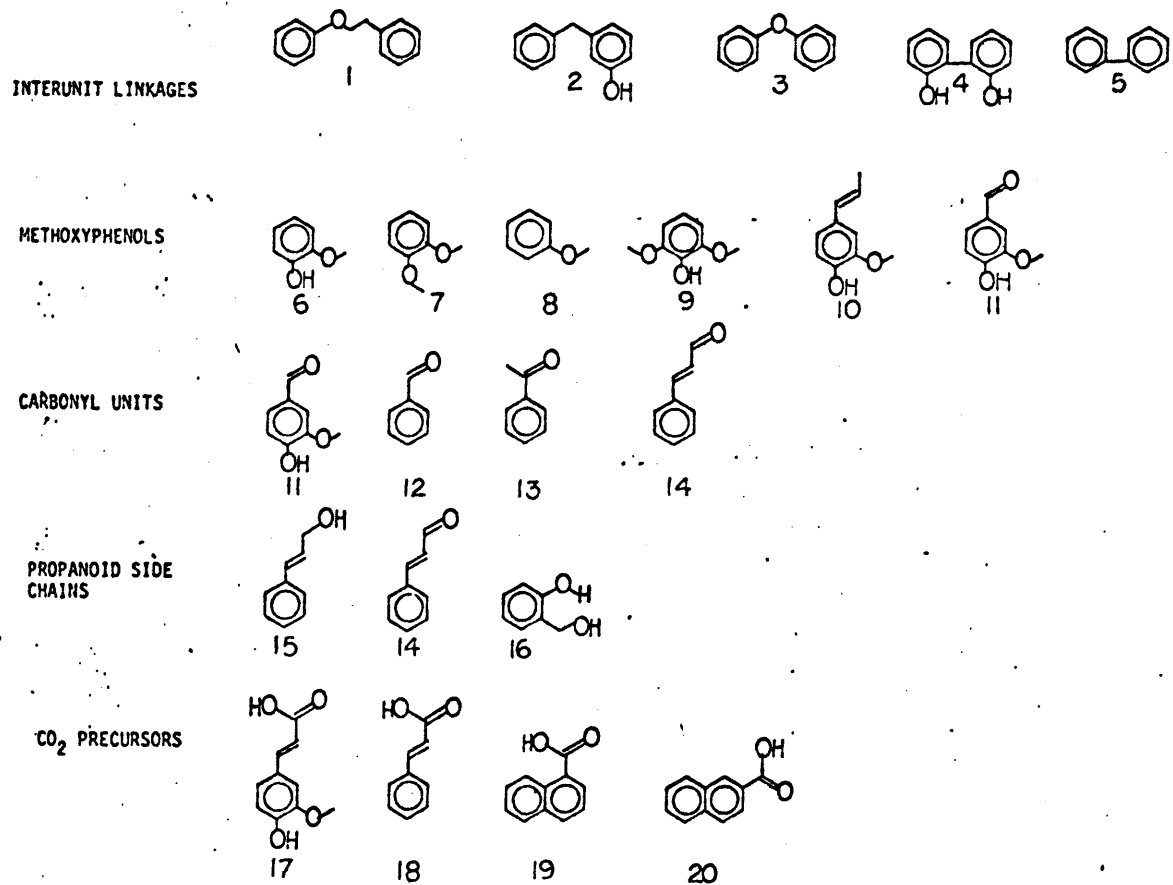
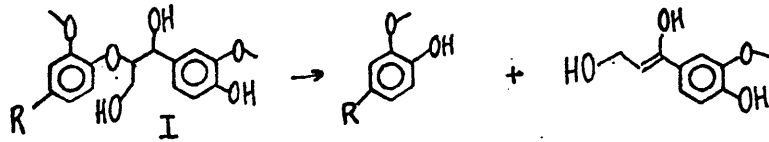


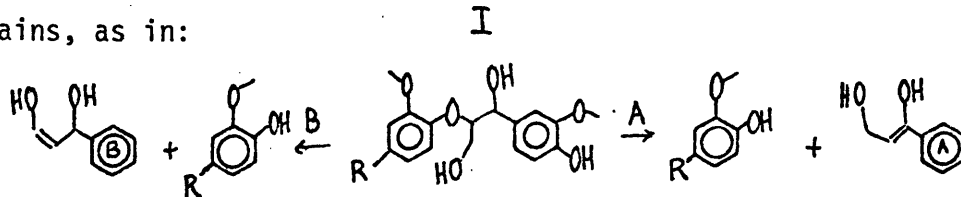
Table 5.1 (cont.) Chemical structure key

methoxyphenol from a veratrole type unit, as in:

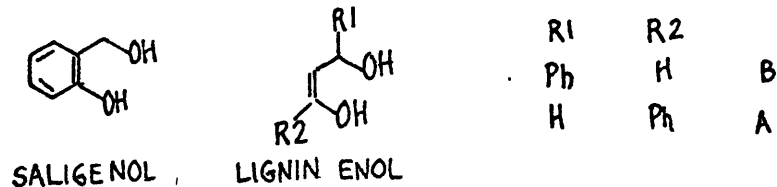


Hence, the relative reactivities of veratrole and guaiacol are of interest.

Reversion of ether I might result in the formation of hydroxy enol side chains, as in:



The hydroxy enol type moiety, IA or IB, is modelled by saligenol, as indicated below:

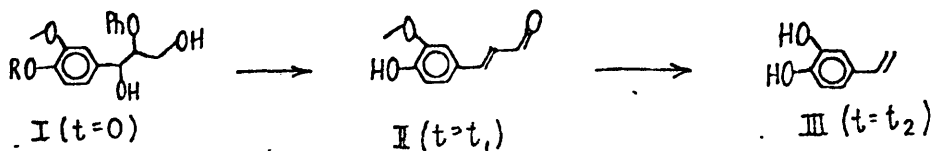


To summarize, the selection of model compounds was effected in two ways. First, compounds which mimic the functionalities and moieties known to exist in the unreacted lignin substrate were selected. The second method of selection was to choose compounds reflecting likely pyrolysis intermediates.

1.5.3 Simulation of Lignin Thermolysis

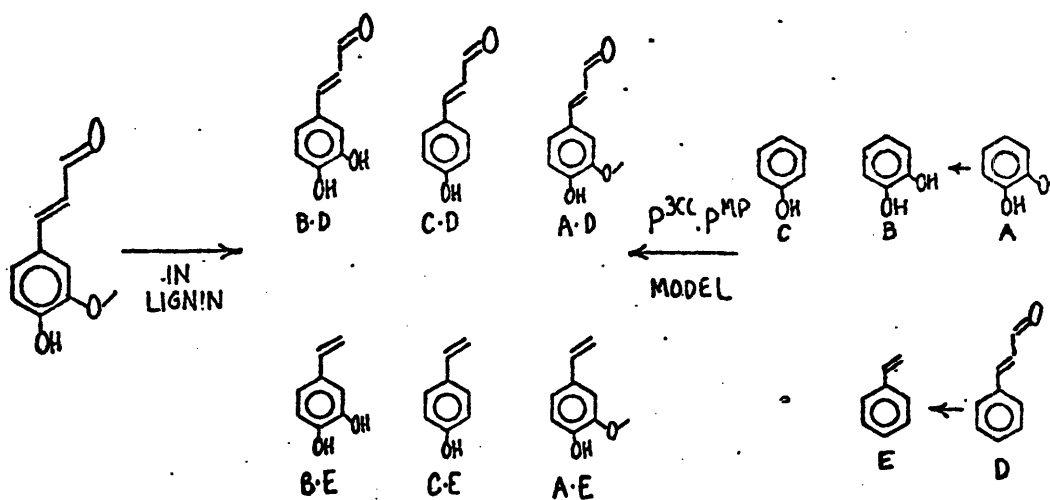
Whole lignin pyrolysis was modelled using the experimental results obtained from the model compound pyrolyses. The task involved depiction of the lignin substrate in terms of the model moieties, followed by delineation of the consecutive and parallel reactions of this substrate in terms of the model pathways. Finally, the products obtained in the model compound pyrolyses had to be related to those of whole-lignin.

Each aromatic unit in lignin was assigned a 3-carbon side chain and methoxyphenol substituent. Consider the structural transformations:



Unit I depicts a typical aromatic unit as found in lignin. Reversion of the β -ether on the side chain followed by subsequent side chain dehydration and methoxyphenol ether cleavage may alter the aromatic unit to II. The original hydroxyl and ether substituents are no longer considered as part of the 3-carbon chain or methoxyphenol, but are either in separate stable products or associated with the 3-carbon chains or methoxyphenol of another aromatic unit. Further reaction could alter the aromatic unit to III. Thus, while the aromatic unit remains intact, changes in the 3-carbon side chain and methoxyphenol substituents chronicle lignin pyrolysis.

The pyrolysis products were then found from a statistical matching of the corresponding products from methoxyphenol and 3-carbon side chain pyrolyses, dictated by the kinetics of each reaction. For example, guaiacol pyrolysis might yield phenol and catechol, whereas cinnamaldehyde might yield styrene. Thus a coniferaldehyde lignin aromatic unit might be expected to yield all of the products shown below. The proportions B:D, C:D, A:D, B:E, C:E, and A:E are dictated by the individual yields of products A through E in experimental pyrolyses of the models guaiacol and cinnamaldehyde. Integration (summation) over the entire distribution of aromatic



units should then describe the products from whole-lignin pyrolysis.

Mathematics of the Simulation

Ordinary linear differential equations describing the variation with time of each methoxyphenol and 3-carbon side chain moiety were used to describe a constant volume batch pyrolysis. The rate of change of each product was, in general, proportional to the number of mols of each other product, or in vector form,

$$\frac{d\vec{X}}{dt} = \underline{\underline{K}}\vec{X} \quad ; \quad \frac{d\vec{Y}}{dt} = \underline{\underline{L}}\vec{Y} \quad \begin{array}{l} \vec{X}(t=0) = \vec{X}_0 \\ \vec{Y}(t=0) = \vec{Y}_0 \end{array}$$

where the vector X represents all methoxyphenol products, and Y is the 3-carbon side chain product vector. The equations were numerically integrated forward in time via a fourth order Runge-Kutta technique. The initial conditions required for the solution of these equations were obtained from the distribution of methoxyphenols and 3-carbon side chains depicted in the Freudenberg structure for spruce lignin, given in Figure 5.2. These conditions reflect the molar, or moiety, fraction of each methoxyphenol or 3-carbon chain in the initial lignin structure. Note that the initial conditions are a function of lignin origin. As light gases, water, and MeOH are evolved in pyrolysis, total simulation mols are not conserved. However, the total number of methoxyphenol and 3-carbon side chain moieties is conserved while being chemically altered in pyrolysis; total aromatic units are also conserved. Formation of single ring aromatic products necessitates that all interunit linkages of the side chain and the methoxyphenols be cleaved. Two types of substituents arise, those entirely free of interunit linkages, designated as S, and those involved in interunit bonding, designated M. Since a single ring aromatic will form only when an S-type 3-carbon chain and an

S-type methoxyphenol are formed, the probability of single ring aromatic formation from lignin, P_S^{LIG} , is $P_S^{LIG} = P_S^{MP} \cdot P_S^{3CC}$. Any other combination involving P_M^{MP} or P_M^{3CC} represents the formation of a multiple aromatic ring product.

In summary, the simulation numerically solved a set of first order differential equations which described the variation with time of the number of each type of 3-carbon side chain and methoxyphenol moiety per unit weight of lignin substrate. The initial concentration of each moiety was obtained from the distributions depicted in the Freudenberg structural model for lignin. Statistical matching of methoxyphenol and 3-carbon side chain substituents at any time then described the products expected from whole-lignin thermolysis.

1.6 Experimental Methods

Table 6.1 is a summary detailing the range of operating conditions for the experimental pyrolyses. Listed are the model compound, structure, purity, and the temperature, time and concentration range studied. The experimental details are conveniently grouped into three categories, namely, the source of the chemicals used for pyrolysis, the actual apparatus used to effect the pyrolyses, and the chemical analysis system used for product characterization.

Chemicals Used

All but one of the compounds were available commercially and were used as received. PPE was not commercially available and this substrate was synthesized by the method of Mademov and Khydyrov¹⁶⁴. Structural details of the synthesis product were confirmed by NMR. Analysis by GC on OV-17 showed the ether to be 95% pure, with phenol, the main impurity, amounting to 1%.

Table 6.1 Experimental Grid for Model Compound Pyrolyses

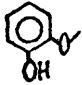
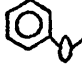
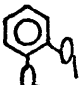
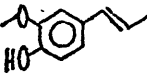
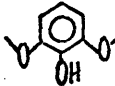
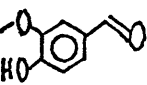
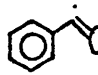
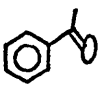
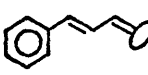
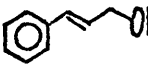
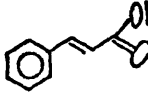
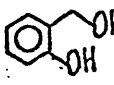

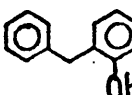

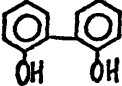
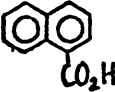
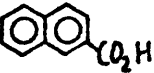
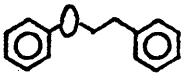
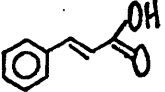
COMPOUND	STRUCTURE	PURITY Wt%	TEMPERATURE RANGE C	HOLDING TIMES s	CONCENTRATION mol/l
GUAIACOL		99	250-535	110-6000	0.46-3.07
ANISOLE		98	344-550	180-1500	0.46-3.07
VERATROLE		98	350-550	60-1500	0.33
ISOEUGENOL		99	300-500	60-1560	0.33
2,6-DIMETHOXY- PHENOL		99	300-500	120-1800	0.32
VANILLIN		99	300-500	120-1500	0.85
BENZALDEHYDE		99	300-500	120-3600	0.16-3.3
ACETOPHENONE		98	350-550	120-4980	0.14-1.4
CINNAMALDEHYDE		99	250-400	120-1500	0.38-1.3
CINNAMYL ALCOHOL		98	300-500	60-1500	0.37-1.1
CINNAMIC ACID		98	300-400	120-1800	.20
SALIGENOL		97	175-350	60-1500	.37
PHENYL ETHER		99	500-587	240-9000	.3
O-HYDROXY- DIPHENYL METHANE		99	400-550	120-6000	.27

Table 6.1 Experimental Grid for Model Compound Pyrolyses (cont'd)

COMPOUND	STRUCTURE	PURITY Wt%	TEMPERATURE RANGE C	HOLDING TIMES s	CONCENTRATION mol/l
BIPHENYL		95	400-587	360-1380	0.40
BIPHENOL		99	400-587	600-1500	.34
1-NAPTHOIC ACID		98	350-450	60-1500	.3±.2
2-NAPTHOIC ACID		99	350-450	60-1500	.3±.2
PHENETHYL PHENYL ETHER		97	300-550	30-14400	0.083-1.68
FERULIC ACID		99	200-350	120-1500	.5

Apparatus

A batch reactor system was employed for all pyrolyses. The batch reactors were stainless steel "tubing bombs" fashioned from Swagelok components. Four different size reactors were used, having volumes of 0.2, 0.6, 3.5, and 10.6 cm³. Kinetic studies were confined to the reactors of 0.2 and 0.6 cm³ in an effort to minimize the effect of heat-up time. The larger reactors were used for quantitative gas and liquid stoichiometry studies.

The batch reactors were either loaded and sealed in a glove box maintained with a nitrogen or argon inert atmosphere, or were externally loaded and slowly purged with an inert flow before closure. The inert served as an internal standard for later gas analyses. Loaded reactors were then immersed in a constant temperature fluidized sand bath for the duration of reaction, and finally quenched in an ice-water bath. After quenching, the reactors were dried, opened, and septum-capped in a helium environment for GC gas analysis. The liquid and solid products were then solvent-collected for later GLC/GC analyses.

Chemical Analysis

The pyrolysis products were identified and analysed by Gas Chromatography. Gases were separated by either molecular sieve(10'), silica gel(6'), or porapak Q(6') columns. Analysis for light liquids, such as H₂O, MeOH, EtOH, and up to about toluene and phenol was effected on porapak Q and principally porapak P(6') columns. The heavier compounds, including alkylbenzenes, phenols and the model compounds were separated on an OV-17 column (6'). Product identification was primarily by GC with standard coinjection. Quantitative product mol fractions were determined from calibration factors obtained from standard samples of known composi-

tion.

1.7 Experimental Results

For each model compound, it was desired to:

1. Characterize and quantify pyrolysis product spectra
2. Develop product relationships and stoichiometries
3. Identify likely reaction pathways
4. Determine reaction orders
5. Measure reaction kinetics and derive Arrhenius parameters.

Experimental results are described for each compound, listed in order of descending importance. Detailed description is limited to Phenethyl Phenyl Ether (PPE) pyrolysis. Kinetic parameters and reaction pathways for each pyrolysis are summarized in Table 1.7.1.

1.7.1 Phenethyl Phenyl Ether (PPE)

The pyrolyses were effected over the range of operating conditions detailed in Table 6.1. The experiments were conducted at temperatures from 300-550 C, with holding times of 1-240 minutes. Substrate conversions were generally held to less than 30% in an effort to emphasize primary reactions; however, kinetic data were obtained at conversions as high as 90%. Initial substrate concentrations ranged from 0.083 to 1.66 mol/l in the gas phase.

PPE was also pyrolysed in tetralin at 350, 400, and 450 C, at substrate concentrations of 0.25mol/l. The effect of tetralin was examined in detail at 400 C, where the mol ratio of tetralin to PPE, called S, was varied from 0.245 to 9.8.

Care was taken to monitor material balance closure, quantified by the determination of the parameter $\langle M \rangle$, physically the average molecular weight of the pyrolysis products, defined below. In this expression X_i is

Table 17.1 Summary of Reaction Pathways and Kinetic Parameters

Substrate	Pathway:Products	$\log_{10} A (s^{-1})$	$E^* (kcal/mol)$
PPE	R1: PhOH + St	11.1	45.0
St	: PhH, To1, EB	5	22
OHD	R1: To1 + PhOH	9.6	43.4
PE	R1: PhH + PhOH	14.8	72.1
BP	R1: 2PhH	-	-
BPhOH	N.R.	-	-
GUA	R1: CAT + CH ₄	10.9	43.7
	R2: PhOH + CO	11.5	47.4
I	R1: PC + CH ₄	10.8	42.9
	R2: PP + CO	11.3	46.2
DMP	R1: MC + CH ₄	10.4	42.2
	R2: GUA + CO	11.1	45.5
VA	R1 _{CH₄} : DHB + CH ₄	12.2	47.3
	R1 _{CO} : GUA + CO	10.2	38.5
VE	R3: GUA + CH ₄	13.9	55.9
	R3': PhOH + CO + CH ₄	14.1	58.4
	R4: AN + CO	14.8	60.1
	R5: oC + CO	11.2	49.2
AN	R3: PhOH + CH ₄	13.0	54.7
	R4: PhH + CO	14.5	61.0
	R5: oC	7.9	40.5
CAL	R1: CAD	14.2	21.8
SAL	R1: QM + H ₂ O	13.4	33.4
BA	R1: PhH + CO	9.5	41.5
AP	: To1	10.9	56.4
	: PhH	9.6	50.5
CAD	R1: St + CO	12.1	48.2
	R2: Phenols	8.5	34.5
	R3: Dimers	8.6	33.7
CA	R1: St + CO ₂	8.0	31.0
FA	R1: VG + CO ₂	5.2	19.8
1-NA	R1: N + CO ₂	4.5	24.0
2-NA	R1: N + CO ₂	7.9	36.5

$$\langle M \rangle \equiv \frac{\sum_{i=2}^n X_i M_i}{\sum_{i=2}^n X_i} \quad \begin{array}{l} n = \text{total number of} \\ \text{products, including} \\ \text{PPE} \\ i=1=\text{PPE} \end{array}$$

the mol fraction and M_i the formula weight of product i . Thus only true products are considered in the $\langle M \rangle$ calculation, with unreacted ether excluded. An ideal production of two product mols from each ether substrate mol would thus yield $\langle M \rangle = 198/2 = 99$. The 157 experimental PPE pyrolyses yielded a mean value $\langle M \rangle = 100.5 \pm 3.98$ as a quantitative measure of pathway closure to two product mols. Carbon, hydrogen and oxygen atom balances were effected and the ratios H/C and O/C were within $\pm 3.2\%$ and $\pm 11.7\%$ of those for the unreacted substrate; the latter provide a measure of overall material balance. The results will be described in two parts, neat pyrolyses and pyrolyses in tetralin.

Neat Pyrolysis

A. Primary Products

The products from representative pyrolyses at various temperatures and times are listed in Table 7.1.1. Two striking observations emerge. First, while 13 pyrolysis products were detected and quantified, the major products were limited to phenol and the hydrocarbons styrene, ethylbenzene, toluene, and benzene. The remaining products, in sum total, amounted to at most 6% of the ether converted. Of the hydrocarbons, styrene was predominant at low conversions, with increasing amounts of toluene as conversion increased. Secondly, the details of the product spectra were relatively insensitive to temperature, and showed a slight dependence on initial substrate concentration and a strong dependence on substrate

E ₀	.25	.25	0.083	0.25	1.66	0.083	0.25	1.66	0.083	0.25	1.66	0.24	0.25
T, C	325	240		400	400		400			400		550	550
t, s	115	40	5	5	5	15	15	15	25	25	25	1	2
E	.9821	.894	.8270	.8863	.869	.5230	.6520	.442	.3900	.417	.2300	.6723	.0207
PhOH	.0603	.064	.0960	.0601	.057	.2420	.1880	.284	.3330	.3040	.3400	.1520	.4000
ST	.0151	.036	.0640	.0375	.044	.1010	.0833	.037	.1020	.0885	.0290	.0876	.1380
T	.0031		.0052	.0102	.0161	.6350	.0373	.0033	.0420	.0813	.1200	.0434	.206
EB	.0077		.0077	.0042	.0057	.0710	.0200	.0584	.1120	.0550	.0980	.0128	.112
S	0		0	.0000	0	0	.0021	.0078	0	.0118	.0160	.0050	.0640
BPE	.0037		0	.0011	.0072	.0054	.0096	.0542	.0075	.0195	.051	.0072	.022
BB	.0004		0	.0006	.0015	.0035	.0060	.0156	.0036	.0164	.0184	.0070	.031
PhTo1	0		0	0	0	.0005	0	.0014	.0008	.0005	.0023	.0001	.0024
PhPhOH	.0008		0	0	0	.0007	0	0	.0007	0	0	.0003	.0083
PhOPh	0		0	0	0	0	0	0	0	.0003	0	.0002	.0020
PH ₂	0		0	0	0	0	0	0	0	0	0	0	.0002
DPM	.0002		0	0	0	0	.0003	.0009	0	.0009	.0015	.0003	.0020
Hvys	0		0	0	0	0	0	0	0	0	0	0	0

Table 7.1.1 Representative product spectra from PPE pyrolysis.

conversion. The latter two observations are reflected most strongly in the relative proportions of major hydrocarbon product.

The time variation of substrate and major product proportions, in mols per initial mol of ether for pyrolysis at 400 C and initial ether concentration of 0.25 mol/l, are depicted in Figure 7.1.1. The slopes of the phenol appearance and ether disappearance are suggestive of a stoichiometric production of phenol from substrate. Figure 7.1.1 further shows the styrene product produced stoichiometrically with phenol at $t=5$ minutes and reaching a maximum at 25 minutes. The maximum yield of styrene, coupled with apparent initial slopes of zero for toluene and ethylbenzene production is suggestive of secondary reactions of the styrene to other products, including toluene, ethylbenzene, and benzene.

The stoichiometric implications of Figure 7.1.1 are further developed in Figure 7.1.2, where product selectivities, i.e., the mol yields of phenol, styrene, and the hydrocarbon sum (styrene+ethylbenzene+toluene+benzene)=(HC) per mol of decomposed substrate, are plotted as a function of substrate conversion. The constant ordinate of unity for phenol at all conversions in Figure 7.1.2 shows that for each mol of ether decomposed a mol of phenol was always produced. For styrene the ordinate decreases monotonically with increasing conversion, from about 0.8 at a fractional conversion of 0.1 to about 0.2 at fractional conversions of 0.8. Thus, at low substrate conversions, one mol of styrene is observed per mol of ether decomposed, but this styrene selectivity decreases with increasing conversion. This is indicative of secondary styrene degradation. Finally, it is observed in Figure 7.1.2 that the hydrocarbon sum HC is essentially unity at all substrate conversions. In summary, then, Figure 7.1.2 shows that decomposition of one mol of ether always yielded one mol of phenol and

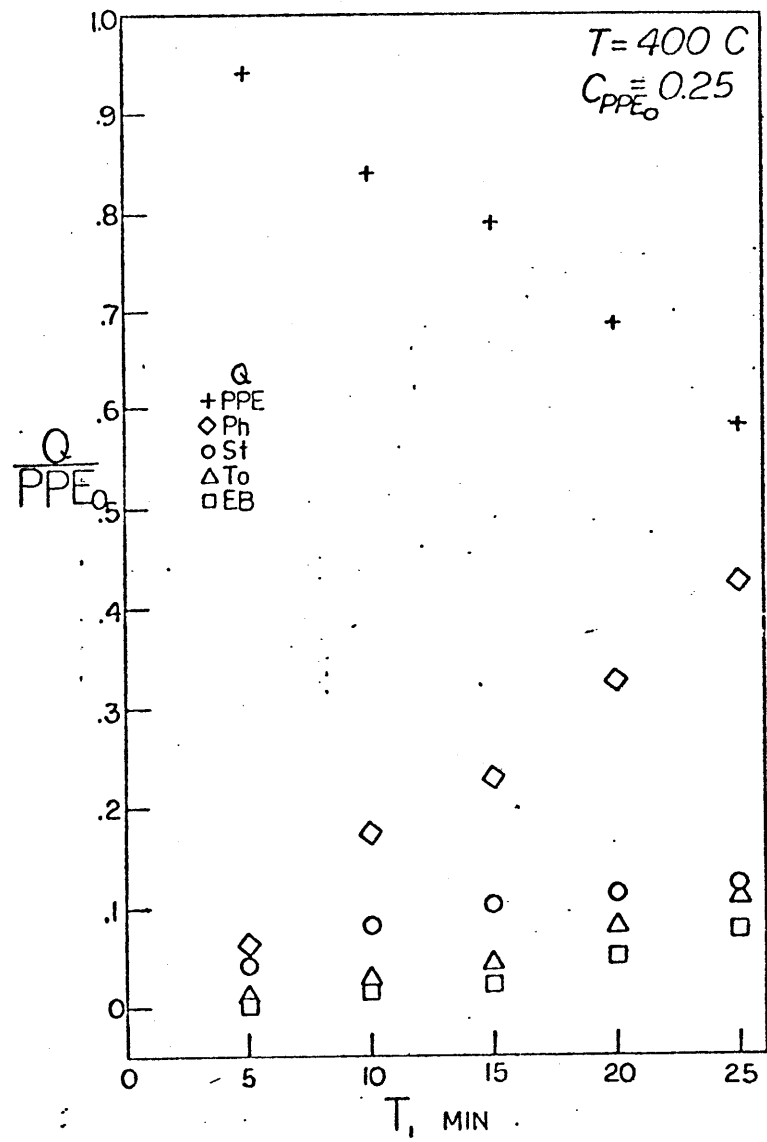


Figure 7.1.1 Major products from neat PPE pyrolysis.

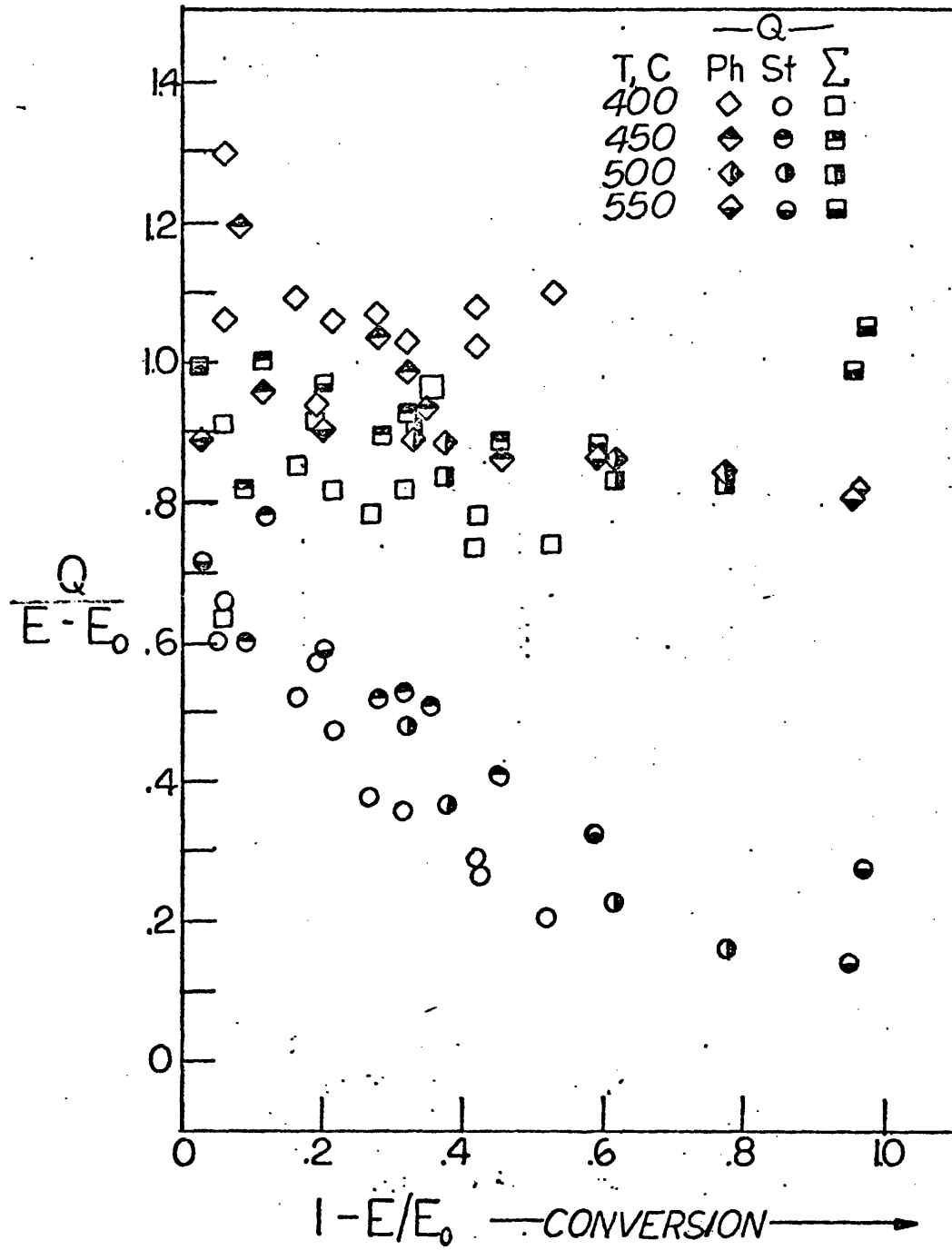
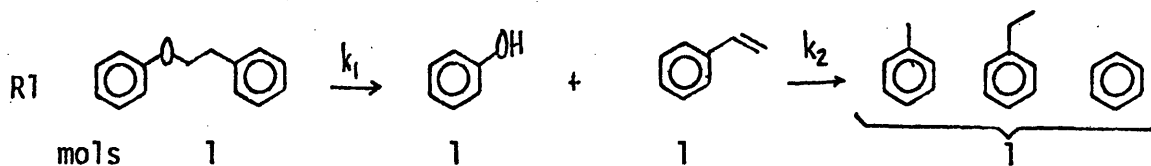


Figure 7.1.2 Product relationships in neat PPE pyrolysis.

one mol of total hydrocarbons. At low substrate conversions, the hydrocarbon is solely styrene, the primary product, which undergoes secondary reactions to the other hydrocarbons at higher conversions. The corresponding pathway for PPE decomposition is the of the type R1:



The order of reaction R1 was examined in a series of experiments at 400 C with initial substrate concentrations ranging from 0.083 to 1.66 mol per liter. Figure 7.1.3 plots the variation with time of $-\ln E/E_0$ for each initial concentration studied, where E is an abbreviated symbol for PPE. A reaction with rate expression $r = kE^\alpha$, i.e., rate constant k and order α , would yield an initial slope $|d \ln(E/E_0)/dt|_{t \rightarrow 0} = kE_0^{\alpha-1}$. The data of Figure 7.1.3 show no systematic dependence on E_0 and are described by a single average slope, implying $\alpha=1$, i.e., first order kinetics. The linearity of $-\ln E/E_0$ vs. t up to fractional conversions of 0.7 is further indicative of first order kinetics. First order rate constants separately determined from Figure 7.1.3 for each initial substrate concentration are plotted in Figure 7.1.4, as $k(\text{s}^{-1})$ versus $E_0(\text{mol/l})$ on doubly logarithmic coordinates. The rate constant is seen to be substantially independent of E_0 over a twentyfold range of the latter.

Further pyrolyses at temperatures from 300-500 C revealed the activation parameters of the first order rate constant. These data are shown in Figure 7.1.5, an Arrhenius diagram with coordinates of $\log_{10} k(\text{s}^{-1})$ vs θ^{-1} , where $\theta = 4.576 \times 10^{-3} T$, with T in Kelvins. On these coordinates, an Arrhenius relationship is described by a straight line $\log_{10} k = \log_{10} A - E^*/\theta$, where the pre-exponential factor A has units of the rate constant

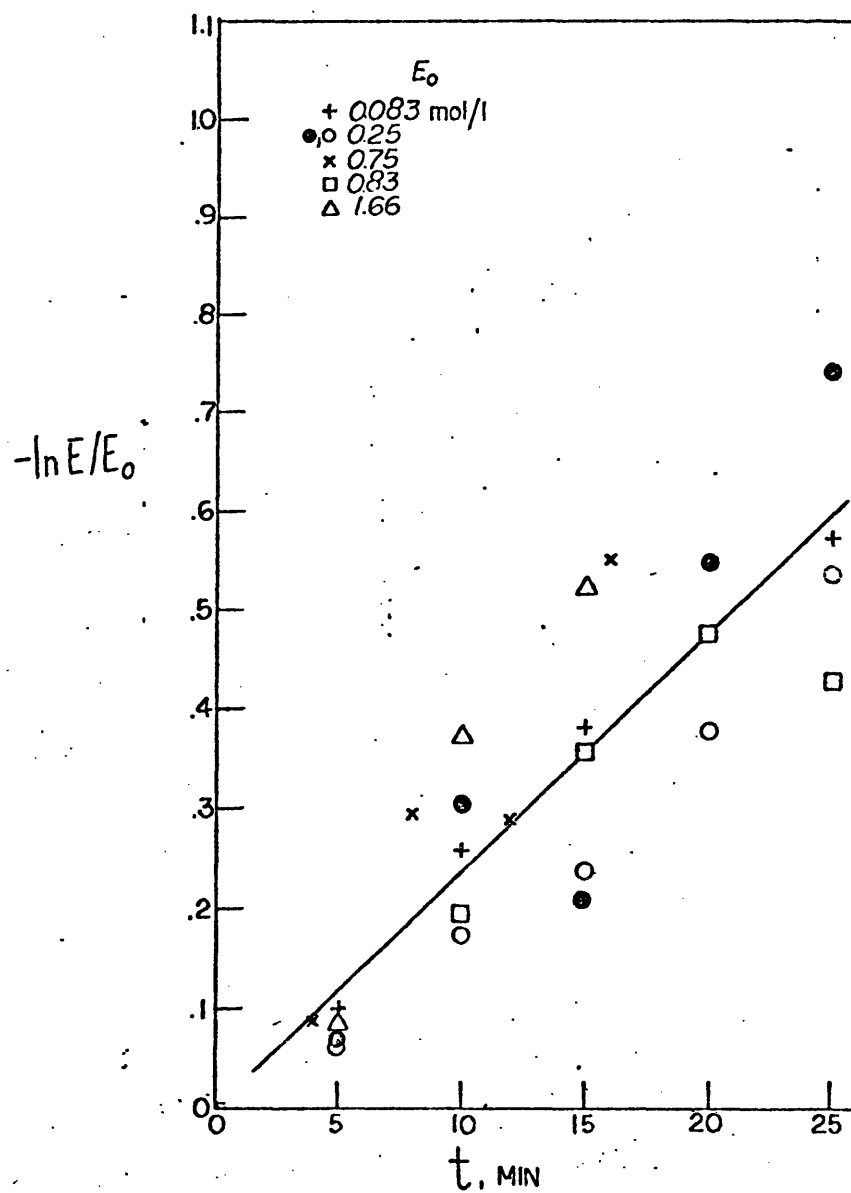


Figure 7.1.3 - PPE pyrolysis kinetics at 400 C.

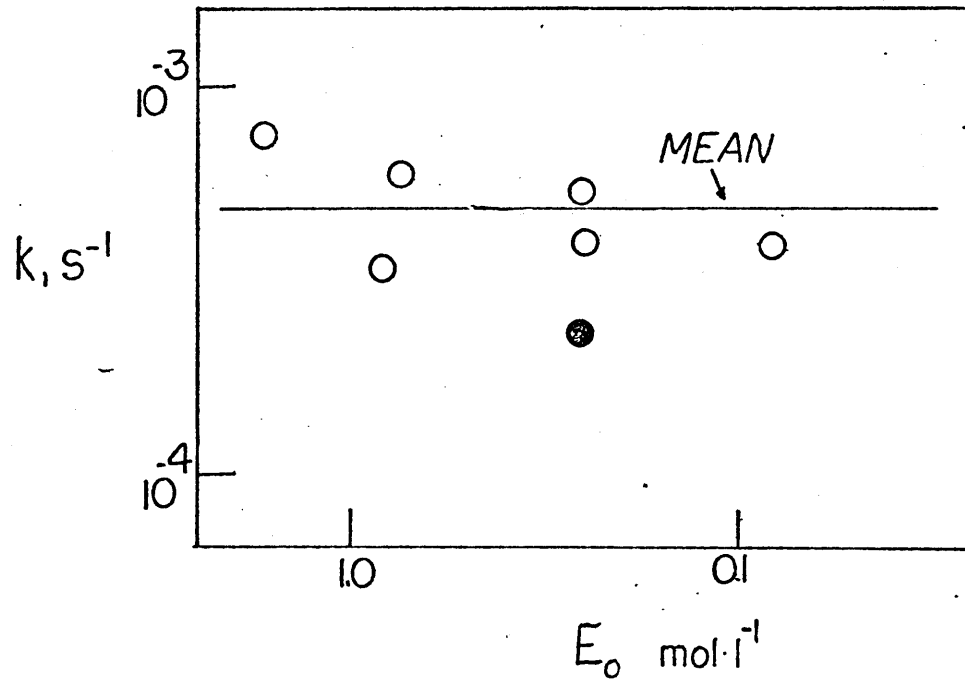


Figure 7.1.4. Variation of k_1^{PPE} with initial PPE concentration

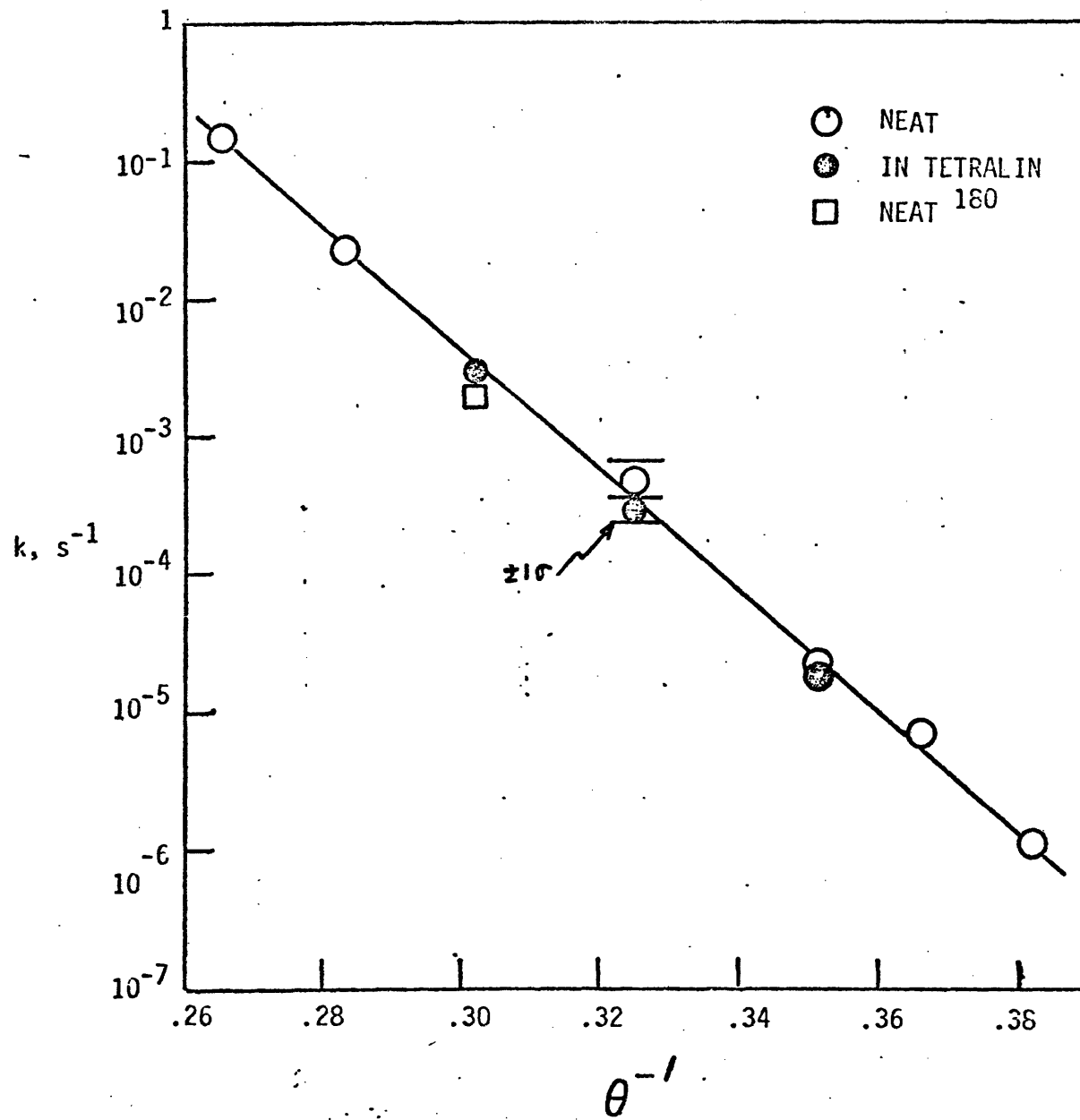


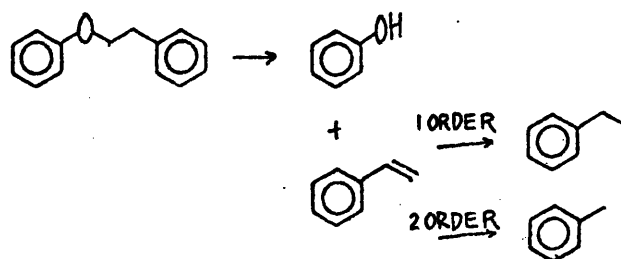
Figure 7.1.5 Arrhenius diagram for PPE pyrolysis.

and the activation energy E^* is expressed in kcal/mol. It is evident from Figure 7.1.5 that $\log_{10}k$ follows the Arrhenius relationship over a range of five orders of magnitude in k . The best fit of these data yields Arrhenius parameters $(\log_{10}A(s^{-1}), E^*(kcal/mol)) = (11.1 \pm 0.9, 45.0 \pm 2.7)$.

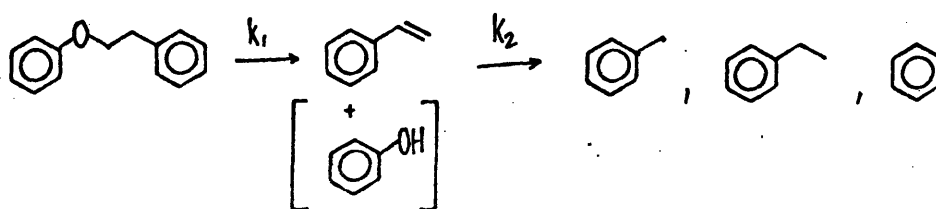
B. Secondary Products

Table 7.1.1 and Figures 7.1.1 and 7.1.2 suggested that ethylbenzene, toluene and benzene were secondary products from styrene degradation. The secondary reaction of styrene was concentration dependent, as depicted in Figure 7.1.6, a plot of product appearance vs. substrate conversion at 400 C for initial PPE concentration, E_0 , ranging from 0.083 to 1.66 mol/l. While the ratios $PhOH/(E_0-E)$ and $HC/(E_0-E)$ were substantially unity, independent of E_0 and substrate conversion, a definite trend of decreasing $St/(E_0-E)$ with increasing E_0 could be discerned at all conversion levels. This is indicative of reaction order in excess of unity for the overall secondary styrene reaction. From Table 7.1.1, the higher order reaction path can be linked with toluene production, which increases with increasing E_0 ; in contrast, the ethylbenzene appearance was relatively insensitive to E_0 . Thus, the pathways to secondary products appear to be

of the type:



The rate for secondary styrene degradation was estimated from the consecutive reaction series:



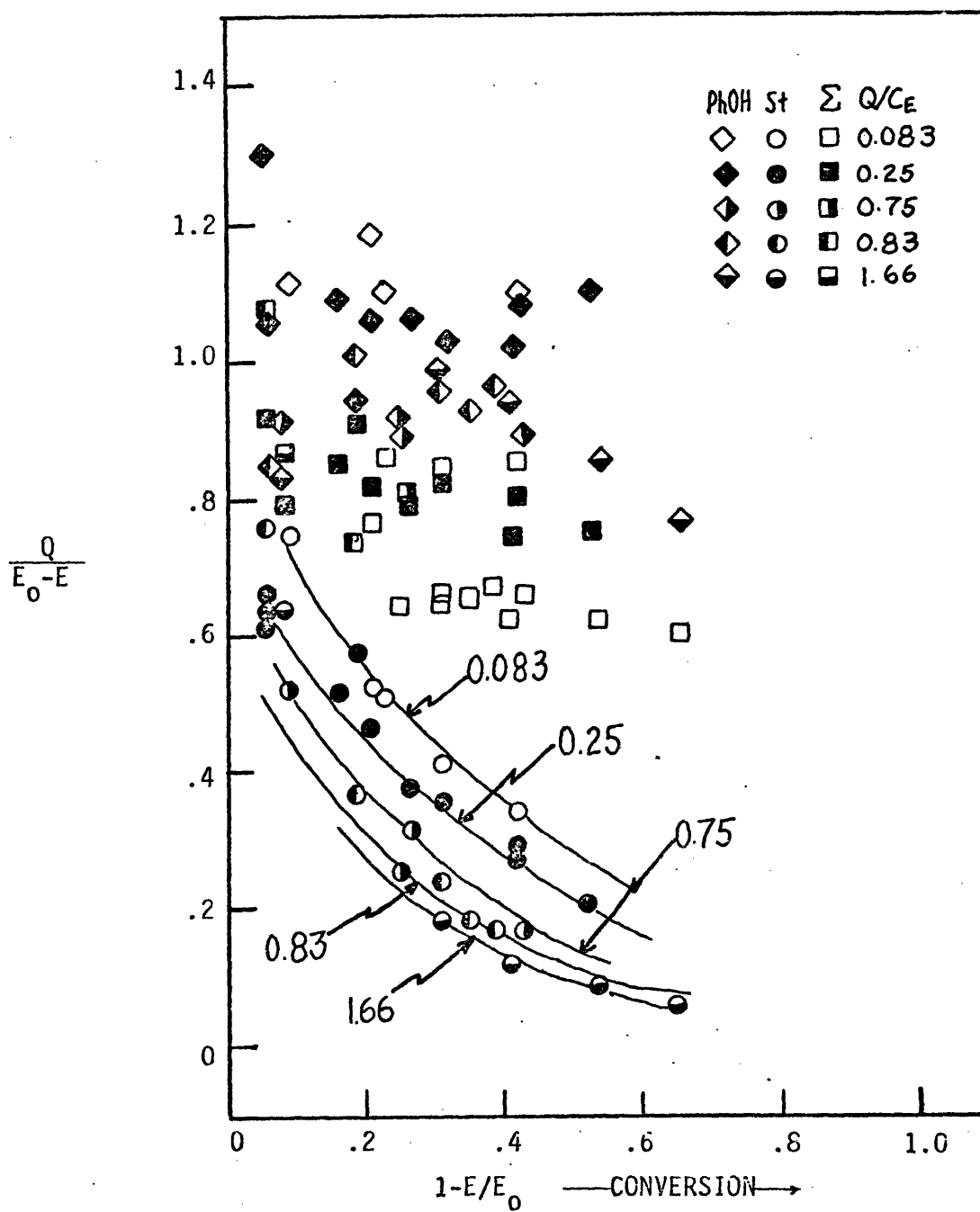


Figure 7.1.6 Product relationships in PPE pyrolysis, T=400 C.

An overall pseudo-first order rate constant k_2 for secondary styrene degradation was obtained from the maximum concentration:

$$\frac{St_{MAX}}{E_0} = \frac{k_1}{k_2} \left(\frac{k_2}{k_2 - k_1} \right)$$

These calculations were made for all PPE pyrolyses where a styrene maximum was apparent, with the results given in Table 1.7.2.

Table 1.7.2 Styrene Pyrolysis Kinetics

T(C)	PPE ₀ (mol/l)	k_2/k_1	k_2 (s ⁻¹)
400	0.083	4.42	0.00172
400	0.25	5.78	0.00310
400	0.25	5.78	0.00225
400	0.75	10.0	0.00585
400	0.83	11.0	0.0037
400	1.66	13.5	0.01
450	0.25	3.15	0.006
500	0.25	2.02	0.018
500	0.75	4.03	0.0655

At a given temperature of 400 C, the ratio k_2/k_1 increased with increasing initial ether concentrations; this reflects the higher order character of styrene degradation relative to ether reversion. The increase in k_2/k_1 with an increase in PPE₀ was also apparent at 500 C. Further, for a given initial ether concentration at 0.25 mol/l, comparison of the data at 400, 450 and 500 C showed that k_2 increased with increasing pyrolysis temperature. The pseudo-first order rate constant k_2 had apparent Arrhenius parameters $(\log_{10} A, E^*) = (5, 22)$; thus, secondary styrene degradation was considerably less activated than the primary reversion of PPE.

Pyrolysis in Tetralin

The ether was pyrolysed in tetralin at temperatures of 350, 400 and 450 C. The primary product spectra were substantially similar to those

for neat ether pyrolysis, as illustrated in Figure 7.1.7, a plot of product yields as a function of reaction time at 400 C, initial tetralin to PPE ratio $S=1.48$, and initial ether concentration $E_0 = 0.25$ mol per liter. The only significant change was in the secondary reaction of styrene, where the presence of tetralin shifted the secondary selectivity toward ethylbenzene. Product relationships were further examined in Figure 7.1.8, where the mol ratios $\text{PhOH}/(E_0-E)$, $\text{St}/(E_0-E)$ and $\text{HC}/(E_0-E)$ are plotted as a function of ether conversion. As was the case with neat pyrolysis, both the ratio $\text{PhOH}/(E_0-E)$ and $\text{HC}/(E_0-E)$ were near unity for all conversions attained, while the ratio $\text{St}/(E_0-E)$ dropped rapidly with conversion. Hence, the primary pathway for ether decomposition to phenol and styrene was unchanged. The rate of styrene decrease was higher in the presence of tetralin than in its absence. Thus, in Figure 7.1.8, the open circles depicting neat pyrolysis indicate a higher styrene concentration at each conversion than do the closed circles representing cases with $S>0$. This is characteristic of a higher order reaction of styrene and tetralin to ethylbenzene, earlier noted as the major secondary pathway for $S>0$.

The kinetics of ether pyrolysis in tetralin were examined for varying values of S at 350, 400, and 450 C. These data are presented in Figure 7.1.9, a plot of the first order rate constant vs. the mol ratio S for each temperature studied. A scale change in the abscissa of Figure 7.1.9 allows inclusion of the rate constant from neat pyrolysis for comparison. At 350 and 450 C rate data were obtained over two orders of magnitude of S . It is evident the rate constants were virtually independent of the presence and amount of tetralin. More comprehensive study at 400 C revealed a slight diminution of the rate constant with increasing

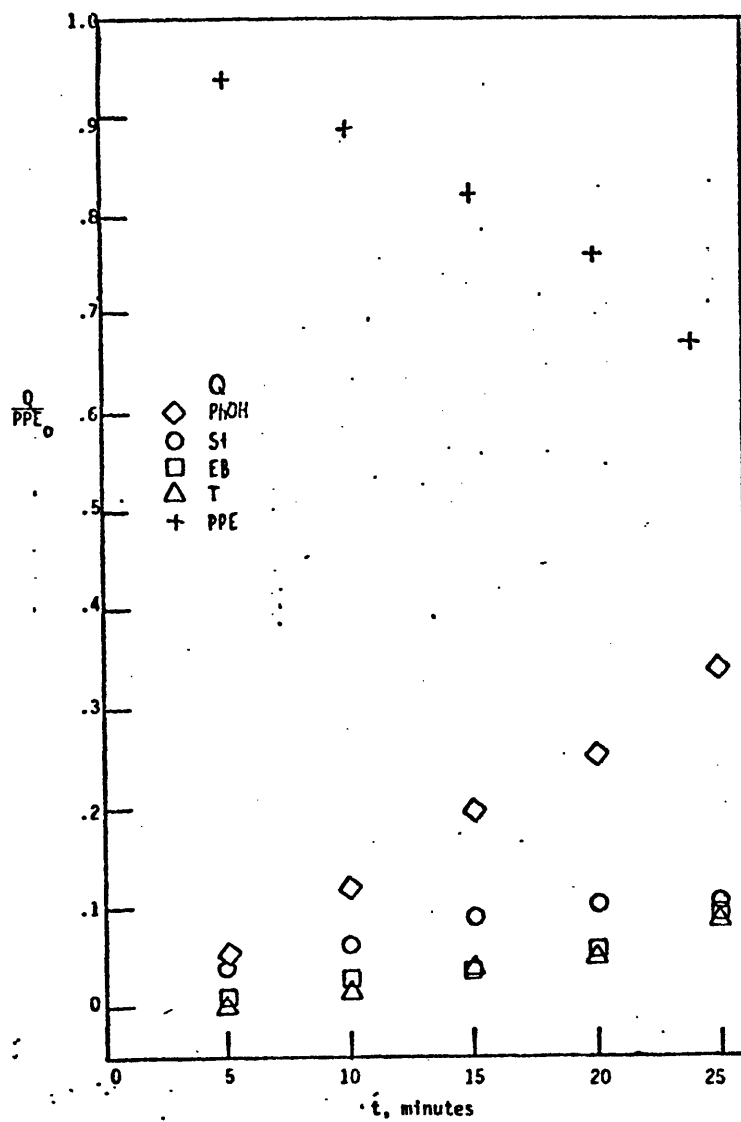


Figure 7.1.7 Major products from PPE pyrolysis in tetralin at 400 C; $C_E=0.25$, $S=1.46$

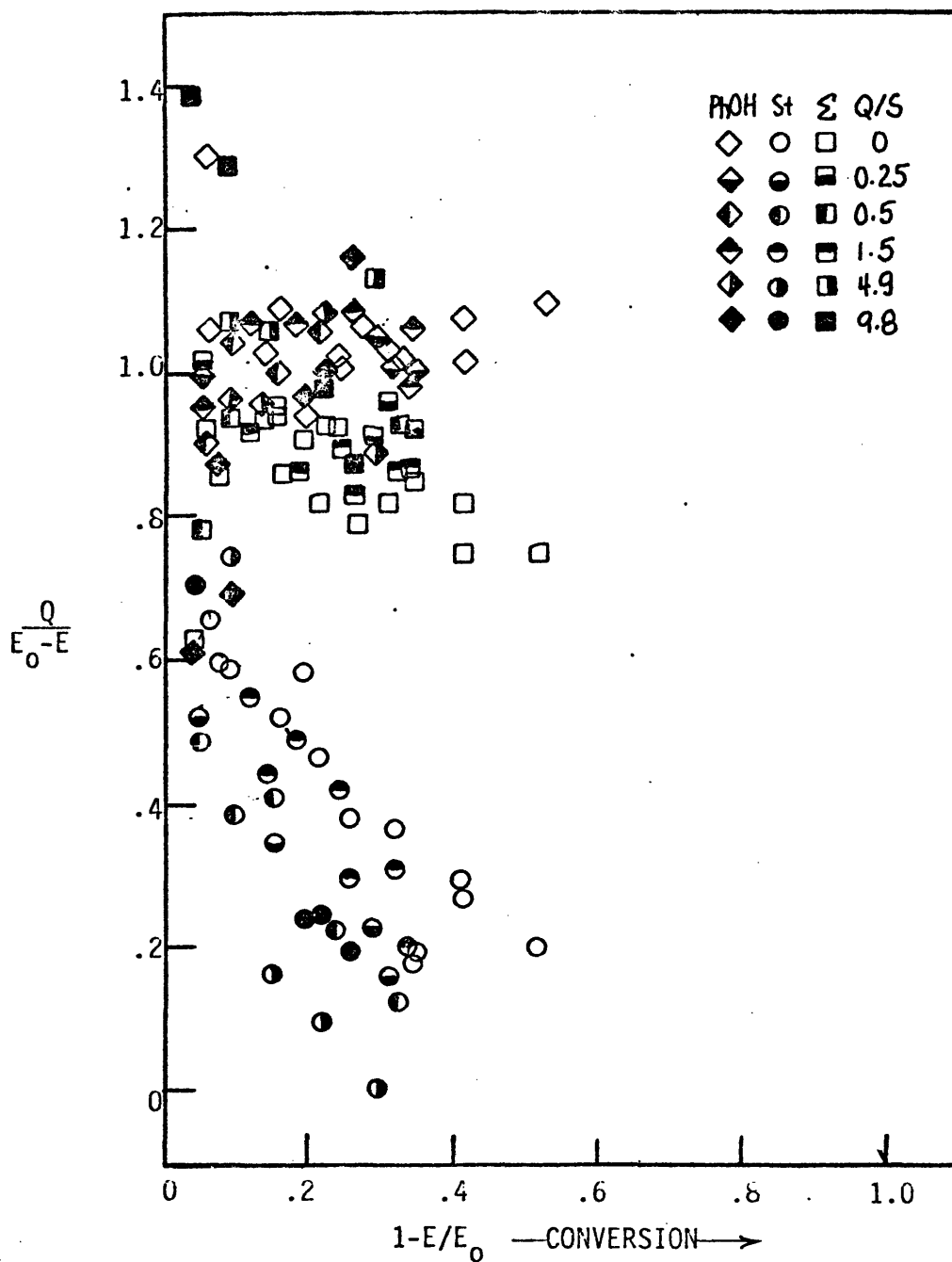


Figure 7.1.8 Product relationships as function of substrate conversion for PPE pyrolysis in tetralin at 400 C.

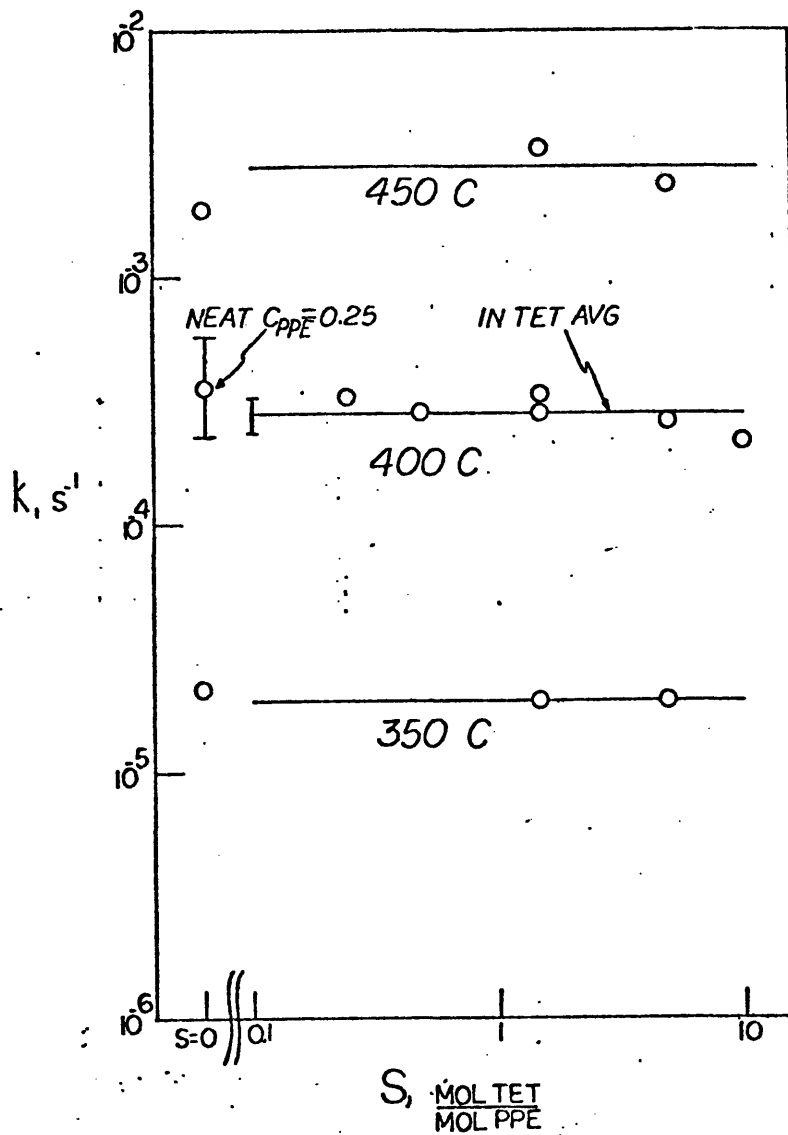


Figure 7.1.9 PPE pyrolysis kinetics, in tetralin

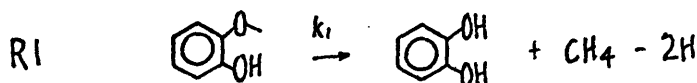
tetralin proportions, of the order of $0.2 \log_{10} k$ units for the range $S=0$ to $S=9.8$. Statistical analyses of the neat and tetralin pyrolyses for all S revealed that the difference in the means of each was less than the standard deviation of this difference. Further comparison of the neat and in-tetralin ether pyrolyses was presented in the Arrhenius diagram Figure 7.1.5. The dark circles representing data for pyrolysis in tetralin were identical with the neat values.

In summary, PPE was pyrolysed both neat and in the presence of tetralin. Neat ether pyrolysis resulted in the primary stoichiometric production of phenol and styrene, with secondary degradation of the latter. Overall ether pyrolysis was substantially first order, and was fit by Arrhenius parameters $(\log_{10} A, E^*) = (11.1, 45.0)$. Secondary pyrolysis of styrene was of reaction greater than unity, and proceeded with apparent pseudo-first order Arrhenius parameters of $(\log_{10} A, E^*) = (5 \pm 2, 22 \pm 3)$. Pyrolysis in tetralin was similar to neat ether pyrolysis, the only significant difference arising as an increased selectivity of secondary styrene conversion to ethylbenzene. The kinetics of neat and in-tetralin pyrolyses were identical.

1.7.2 Summary of Experimental Results

Guaiacol

Two parallel pathways described guaiacol pyrolysis, these being demethanation to catechol and methane and demethoxylation to phenol and CO.



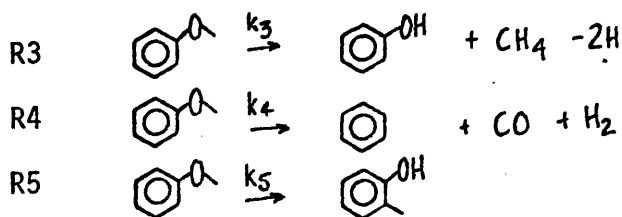
The former pathway was tenfold faster. The assignment of catechol as a direct pyrolysis product is as yet tentative. Both of the demethanation and

demethoxylation pathways were first order in substrate, with respective Arrhenius parameters ($\log_{10} A, E^*$) = (10.9±0.5, 43.7±1.4) and (11.5±0.5, 47.4±1.6).

Substituted Guaiacols: 2,6-dimethoxyphenol (DMP), Isoeugenol, Vanillin
 Pyrolyses of DMP, isoeugenol, and vanillin probed the respective effects of electron donating, conjugative, and electron withdrawing substitution on guaiacol reactivity. The substrates decomposed by pathways similar to R1 and R2 for guaiacol; vanillin underwent extensive decarbonylation as well. The kinetics of guaiacol demethanation and demethoxylation were virtually unaffected by substitution.

Anisole

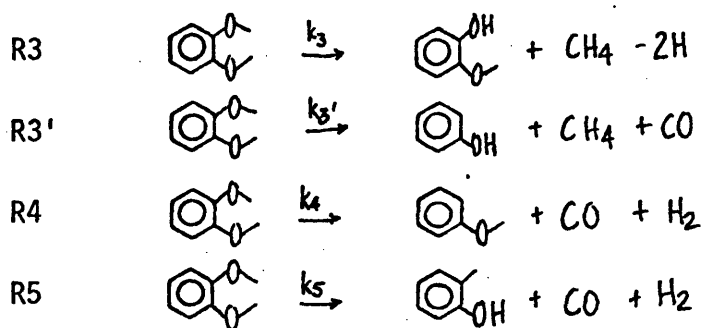
Anisole pyrolysis probed the effect of ortho-hydroxy substitution on the reactions of the guaiacol methoxyl group. The effect is marked, as overall anisole pyrolysis was typically at least an order of magnitude slower in rate than that of guaiacol. Three pathways described anisole pyrolysis, leading to the formation of phenol, benzene, and o-cresol:



Unequivocal relationships between gas and liquid phase products could not be discerned. First order Arrhenius parameters were ($\log_{10} A, E^*$) = (13.0±1.0, 54.7±3.1), (14.5±1.2, 61.0±4.0), and (7.9±1.5, 40.5±4.9) for R3, R4, and R5, respectively.

Veratrole

Four primary reaction pathways were important in veratrole pyrolysis. These were similar to those previously described for anisole, and took the form listed below. The kinetics of pathways R3 and R5 were compar-



able to those for analogous R3 and R5 anisole pathways. Apparent first order Arrhenius parameters ($\log_{10} A, E^*$) = (13.9 ± 1.3, 55.9 ± 4.0), (14.1 ± 1.0, 58.4 ± 2.8), (14.8 ± 1.8, 66.1 ± 5.7) and (11.2 ± 2.2, 49.2 ± 7.1) for pathways R3, R3', R4, and R5, respectively.

Saligenol

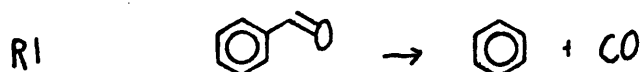
Saligenol underwent facile dehydration at temperatures as low as 175–225 C. Each mol of decomposed substrate yielded one product mol of water. Thus, a pathway of the type R1 was postulated, where:



The quinonemethide was not isolated, being a labile precursor to the only major pyrolysis co-product, an obscure higher molecular weight polymer. Apparent first order Arrhenius parameters for R1 were ($\log_{10} A, E^*$) = (13.4 ± 2.9, 33.4 ± 6.3).

Benzaldehyde

The major pyrolysis route for benzaldehyde was first order degradation to stoichiometric amounts of CO and benzene, pathway R1:

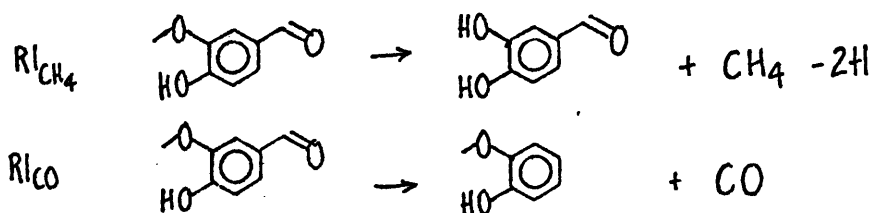


Kinetic description of R1 at temperatures from 300–500 C provided first

order Arrhenius parameters $(\log_{10} A, E^*) = (9.5 \pm 0.8, 41.5 \pm 2.7)$.

Vanillin

Vanillin pyrolysis involved two major pyrolysis pathways, demethanation to dihydroxybenzaldehyde and decarbonylation to guaiacol; the latter pathway was faster by a factor of 10. Thus, vanillin pyrolysis pathways were of the type R1 previously delineated for each of guaiacol and benzaldehyde. Kinetic analysis of vanillin pyrolysis yielded de-



methanation parameters of $(\log_{10} A, E^*) = (12.2 \pm 3.0, 47.3 \pm 8.6)$ and decarbonylation parameters of $(10.2 \pm 2.1, 38.5 \pm 5.9)$. Thus, guaiacol demethanation was essentially unaffected by carbonyl substitution, whereas benzaldehyde decarbonylation was markedly enhanced by guaiacyl substitution.

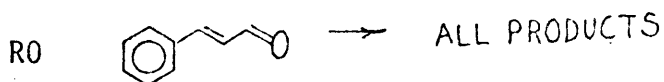
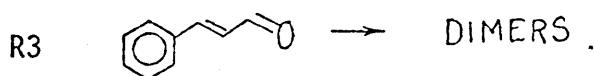
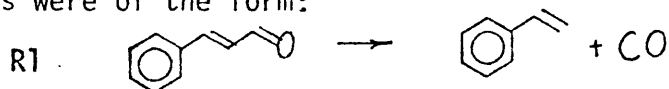
Acetophenone

Acetophenone pyrolysis yielded CO , CH_4 , benzene and toluene as the major light products, along with appreciable amounts of alkylbenzenes, phenols and apparent dimers. Because of the complexity of the liquid product spectra, no clear link could be established between gaseous and condensed phase products. An apparent overall acetophenone decomposition reaction order of 1.2-1.3 was determined, with a reaction order of unity for toluene appearance and 1.5 for benzene appearance. Pseudo-first order Arrhenius parameters for overall acetophenone decomposition, benzene appearance and toluene appearance were $(\log_{10} A, E^*) = (10.9 \pm 1.2, 52.1 \pm 4.1)$, $(9.6 \pm 1.9, 50.5 \pm 6.7)$ and $(10.9 \pm 2.2, 56.4 \pm 7.6)$, respectively. Overall acetophenone pyrolysis was typically two orders of magnitude slower than benz-

aldehyde pyrolysis for the temperature range studied here.

Cinnamaldehyde

Pyrolysis of cinnamaldehyde yielded styrene, phenols, apparent dimers, and CO as primary products, as well as toluene and ethylbenzene as secondary products. Styrene and CO were formed stoichiometrically at low substrate conversions. Overall cinnamaldehyde decomposition was described in two parts, a set of first and a set of second order reactions, of the form: $-d(\text{CAD})/dt = k_1(\text{CAD}) + k_2(\text{CAD})^2$, where k_1 accounts for first order reactions and k_2 the second order reactions. Styrene and phenol appearance were best described as first order, and dimer formation by a reaction order in excess of unity, likely two. The major cinnamaldehyde pyrolyses were of the form:

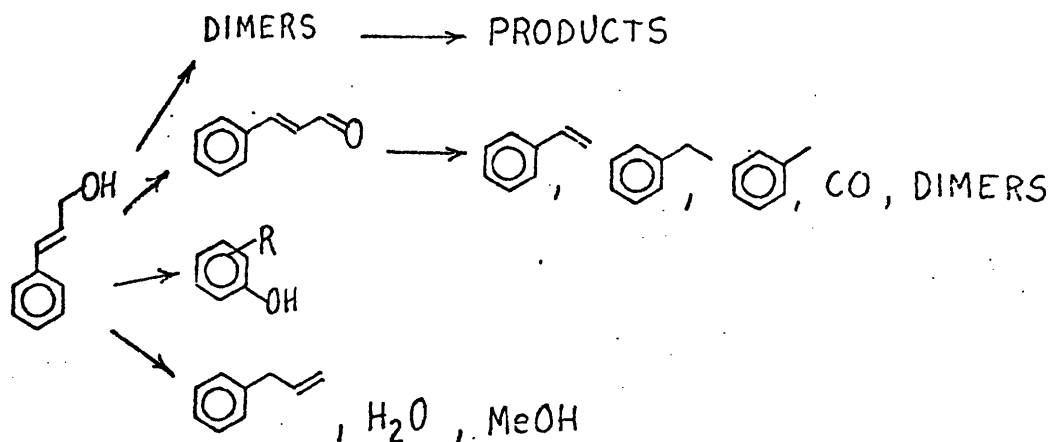


Pseudo-first order Arrhenius parameters for R1, R2, R3, and R0 were $(\log_{10} A, E^*) = (12.1 \pm 0.4, 48.2 \pm 1.1), (8.5 \pm 0.4, 34.5 \pm 1.0), (8.6 \pm 1.4, 33.7 \pm 3.1)$ and $(9.7 \pm 1.7, 35.4 \pm 4.6)$, respectively.

Cinnamyl Alcohol

The products from cinnamyl alcohol pyrolysis fell into one of four categories: a gas fraction, water soluble light liquids, monoaromatics, and a polymeric fraction. Significant products were CO, H₂O, MeOH, cinnamaldehyde, styrene, phenols, allylbenzene, and apparent dimers. In spite of

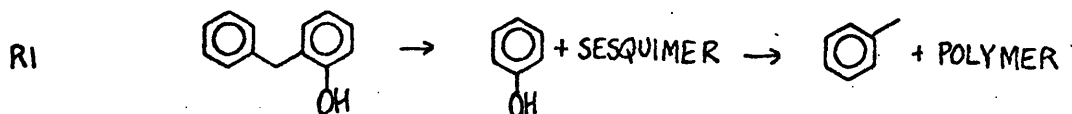
complex product spectra, several generalizations regarding cinnamyl alcohol pyrolysis were possible. Lower temperature pyrolysis data suggested that dimers, cinnamaldehyde, phenols, allylbenzene, water and methanol were primary products, whereas styrene, toluene, ethylbenzene, and CO likely arose from secondary pyrolyses. The reaction network was of the type:



Of the primary reactions, cinnamaldehyde, dimer and alkylphenol formation were the most facile, whereas methanol formation was typically two orders of magnitude slower in rate than overall alcohol decomposition.

Orthohydroxydiphenylmethane (OHD)

Pyrolysis of OHD resulted in phenol, toluene, and apparent triphenyl sesquimers as the major products. Of these, phenol and sesquimers were primary, the latter degrading by secondary pathways to toluene. OHD degradation pathways were of the type R1:



Apparent first order Arrhenius parameters for OHD pyrolysis were ($\log_{10} A$, E^*) = (9.6±0.4, 43.4±1.4).

Phenyl Ether

The pyrolysis of phenyl ether could be effected only at temperatures in excess of 500 C. The major pyrolysis products were phenol, benzene, and apparent sesquimers. Ether pyrolysis appeared to proceed via primary degradation to phenol and sesquimers, the latter capable of degradation to benzene and polymers. Thus, a pathway of the type R1 was suggested, where :



Apparent first order Arrhenius parameters were $(\log_{10} A, E^*) = (14.8 \pm 1.3, 72.1 \pm 4.8)$.

Biphenyl

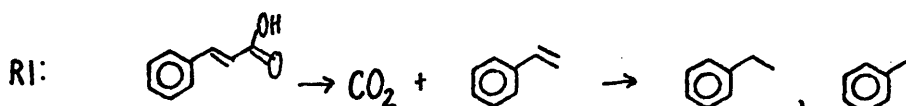
Pyrolysis of biphenyl to benzene occurred only at 587 C. Higher molecular weight materials, which were presumably formed to maintain hydrogen balance, went undetected in the present analysis. An apparent first order rate constant $-\log_{10} k_{587 \text{ C}} = 3.82$ was determined.

Biphenol

Biphenol was pyrolysed to 500 C and 30 minutes holding time. The compound was quite stable, and no degradation to any light products could be discerned.

Cinnamic Acid

Pyrolysis of cinnamic acid over a temperature range of 300-400 C produced CO_2 and styrene as major primary products, the latter capable of secondary degradation to toluene and ethylbenzene. The major cinnamic acid pathway was thus of the type R1, namely:



Apparent first order Arrhenius parameters of $(\log_{10}A, E^*) = (8.0 \pm 1.8, 31.0 \pm 5.0)$ were determined.

Ferulic acid

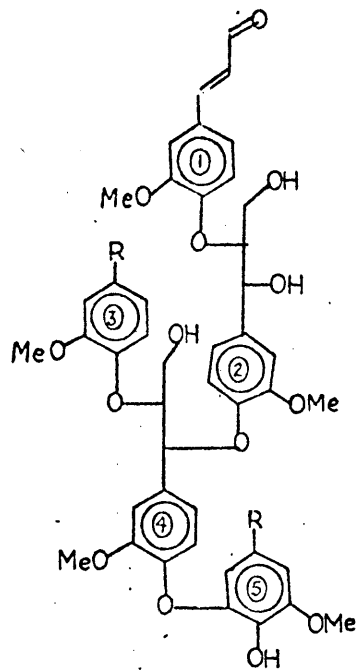
Pyrolysis of ferulic acid from 200-350 C elucidated the effect of guaiacyl substitution on cinnamic acid decarboxylation. Initial rates of CO_2 release were a hundred fold higher for ferulic acid than for cinnamic acid, showing substantial decarboxylation enhancement by guaiacyl substitution. Apparent first order rate data from the initial rates of CO_2 formation yielded Arrhenius parameters of $(\log_{10}A, E^*) = (5.2 \pm 2.0, 19.8 \pm 5.2)$.

Napthoic Acids

The time evolution of CO_2 from 1- and 2- napthoic acids was monitored from pyrolyses at 300, 400, and 500 C. The pyrolyses were modelled as a stoichiometric evolution of CO_2 and naphthalene. CO_2 release from 1-napthoic acid was faster than that from 2-napthoic acid. Apparent first order Arrhenius parameters of $(\log_{10}A, E^*) = (4.5 \pm 1.4, 24.0 \pm 1.3)$ and $(7.9 \pm 2.7, 36.5 \pm 8.1)$ were determined for 1- and 2- napthoic acids, respectively.

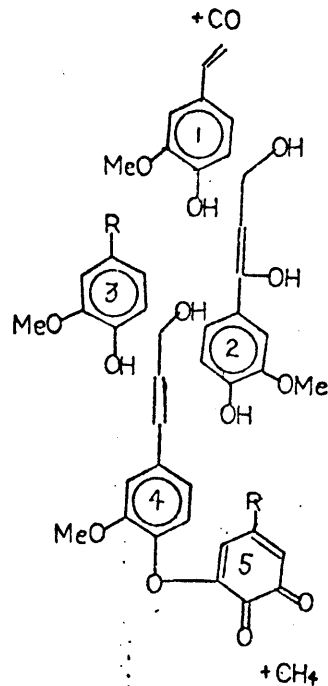
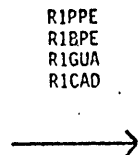
1.8 Implications of Experimental Results

The model compound pyrolysis pathways developed in the previous section allowed formulation of a primary reaction network to describe the essential features of lignin pyrolysis. The network is presented as Figure 8.1. For illustrative purposes, lignin has been depicted as the oligomeric unit I. The primary reactions used in Figure 8.1 are PPE reversion, BPE cleavage, guaiacol demethanation, and cinnamaldehyde decarbonylation. The veratrole methoxyls of aromatic units 1, 2, 3, and 4 are considered unreactive. Among the interunit linkages, the diphenyl-ether between units 4 and 5 is inert. Application of the facile guaiacol,



I

	current	net
CH ₄	0	0
CO	0	0
H ₂ O	0	0
H ₂	0	0



II

	cur	net
CH ₄	1	1
CO	1	1
H ₂ O	0	0
H ₂	0	0

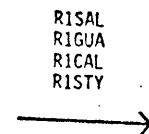
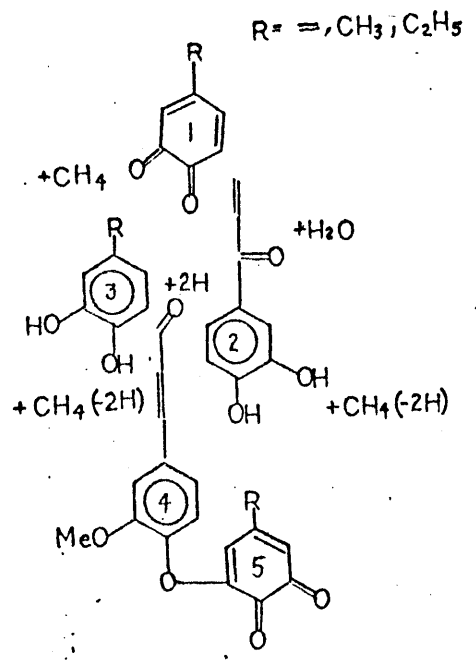
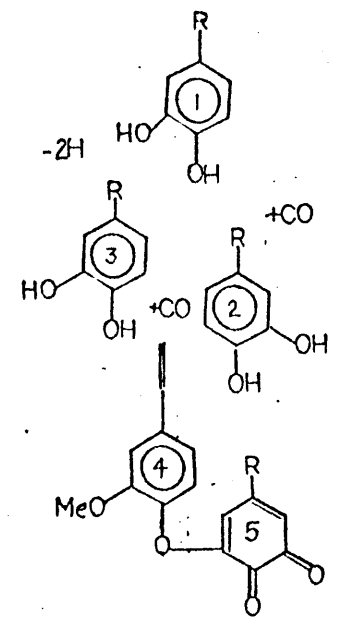


Figure 8.1 Model pathway for lignin pyrolysis.



RICAD
RIGUA

→



	cur	net
CH ₄	3	4
CO	0	1
H ₂ O	1	1
H ₂	-1	-1

	cur	net
CH ₄	0	4
CO	2	3
H ₂ O	0	1
H ₂	-1	-2

Figure 8.1 (cont)

cinnamaldehyde, PPE, and BPE R1 pathways to structure I generates the structures shown as set II. The cinnamaldehyde reaction of unit I released CO and generated a styrene side chain. Reversion of PPE and BPE links resulted in guaiacol formation at units 1, 2, and 3, as well as a saligenol moiety on unit 2 and a cinnamyl alcohol on unit 4. Demethanation resulted in the formation of a diquinone at unit 5. The net release of gases and water is tabulated in Figure 8.1; one mol each of CO and CH₄ were formed in transformation of the lignin depicted as structure I to set II. The aromatics generated in set II are subject to further reactions, resulting in the products shown as set III. With regard to set III, unit 1 depicts guaiacyl demethanation as well as the degradation of styrene to toluene, ethylbenzene, and benzene. The products from whole-lignin pyrolysis, then, would be catechol, methylcatechol, and ethylcatechol precursors. Units 2 and 3 similarly depict guaiacyl demethanation, greatly facilitated by ether reversion. Water arose from dehydration of the saligenol moiety of unit 2, which generated the guaiacyl acrolein as well. Unit 4 depicts cinnamyl alcohol dehydrogenation to cinnamaldehyde; it also illustrates the relative stabilities of the phenyl ether link and thus of the associated veratrole methoxyl. Further application of the same kinds of reactions to set III generates the compounds of set IV, of which some may still further react. However, the veratrole methoxyl of unit 4 is relatively stable, and the diphenylether is essentially inert; both will thus concentrate in the carbonaceous residue.

The structural moieties and possible reactions of Figure 8.1 depict only a small number of the pathways involved in whole-lignin pyrolysis. A more accurate description of lignin pyrolysis must incorporate more of the structural details of the Freudenberg model as well as account for the

complex set of parallel and consecutive reactions likely important in lignin pyrolyses. For this purpose, a lignin pyrolysis simulation model was developed. This model combined the approach outlined in section 1.5 with the experimental model compound pyrolysis results. It possessed the same logic as displayed in Figure 8.1, but was considerably extended in scope.

1.9 Simulation Results

Spruce lignin pyrolysis was simulated at temperatures of 300, 400, 500, and 600 C, to holding times of 10^4 , 10^4 , 10^2 , and seven seconds, respectively. Figures 9.1a, b, and c are graphical presentations of selected product yields at each temperature studied. The present discussion will consider the more important aspects of these simulation results, which will be described in terms of the gas, light liquid, phenolic, and carbonaceous coke product fractions.

1.9.1 Gas Evolution

The model presently accounts for methane and carbon monoxide release.



Simulated pyrolysis to 10^4 s produced methane in yields of 0.05% and 6.2% at 300 and 400 C, respectively. The greater yield at 400 C reflects not only guaiacol and veratrole activation, but also activation of the prevalent PPE linkage. At 500 C and 100 s, the simulation predicted a methane yield of 5.9%, whereas at 600 C and 7s, a yield of 6.1% was predicted. Thus, these increases in the pyrolysis temperature resulted in a sharp decrease in the time required to reach a nominal yield of 6%. These yields compare with a theoretical maximum of about 9%, obtained by assuming each aromatic unit could contribute one methane mol.



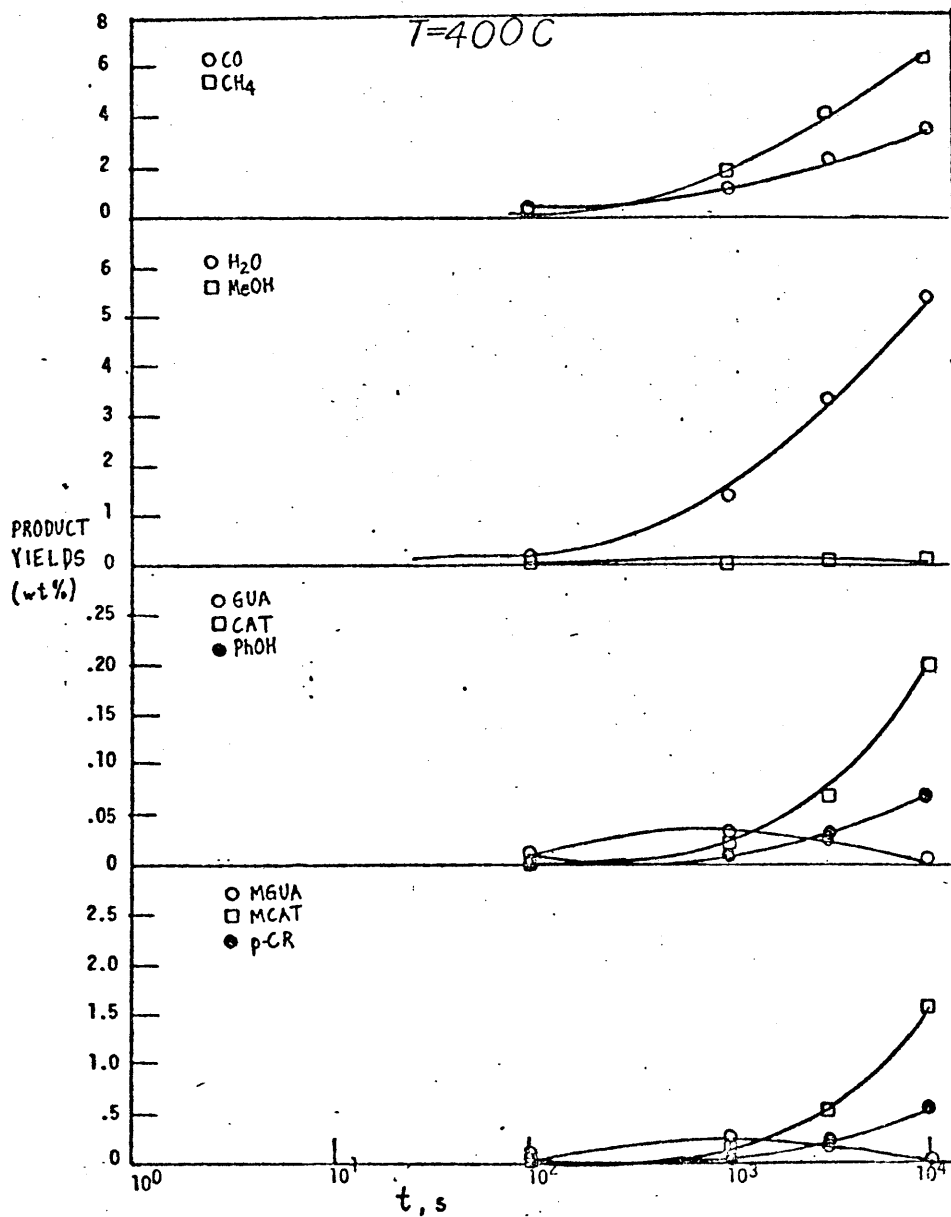


Figure 9.1a Model predictions at 400 C.

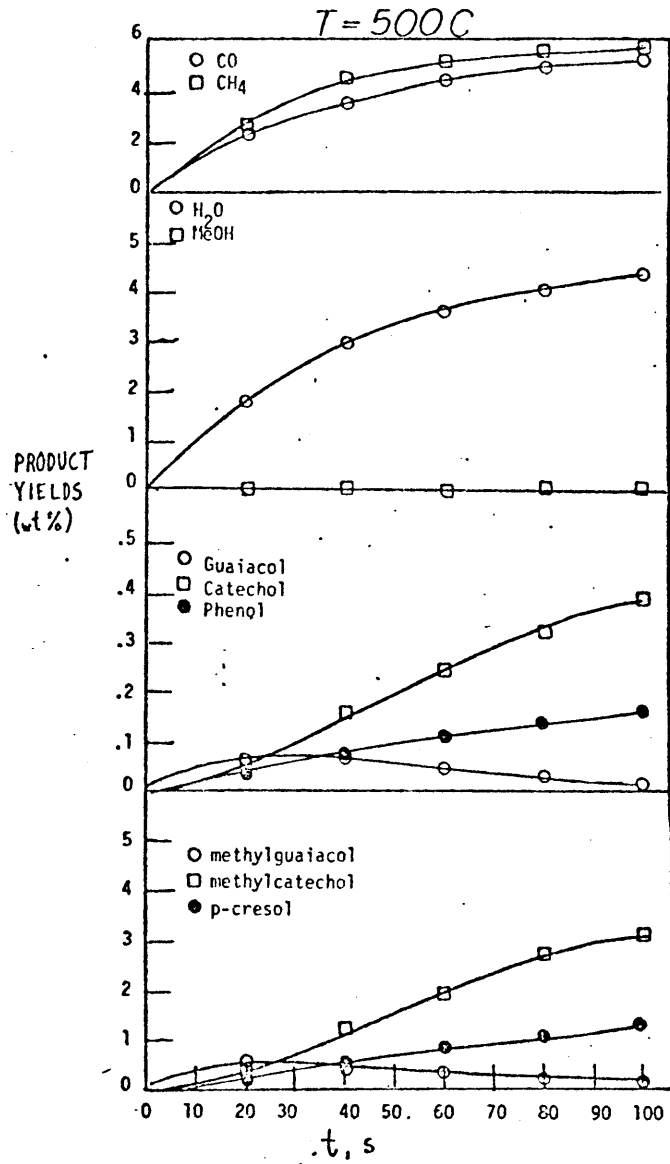


Figure 9.1b Model predictions at 500 C.

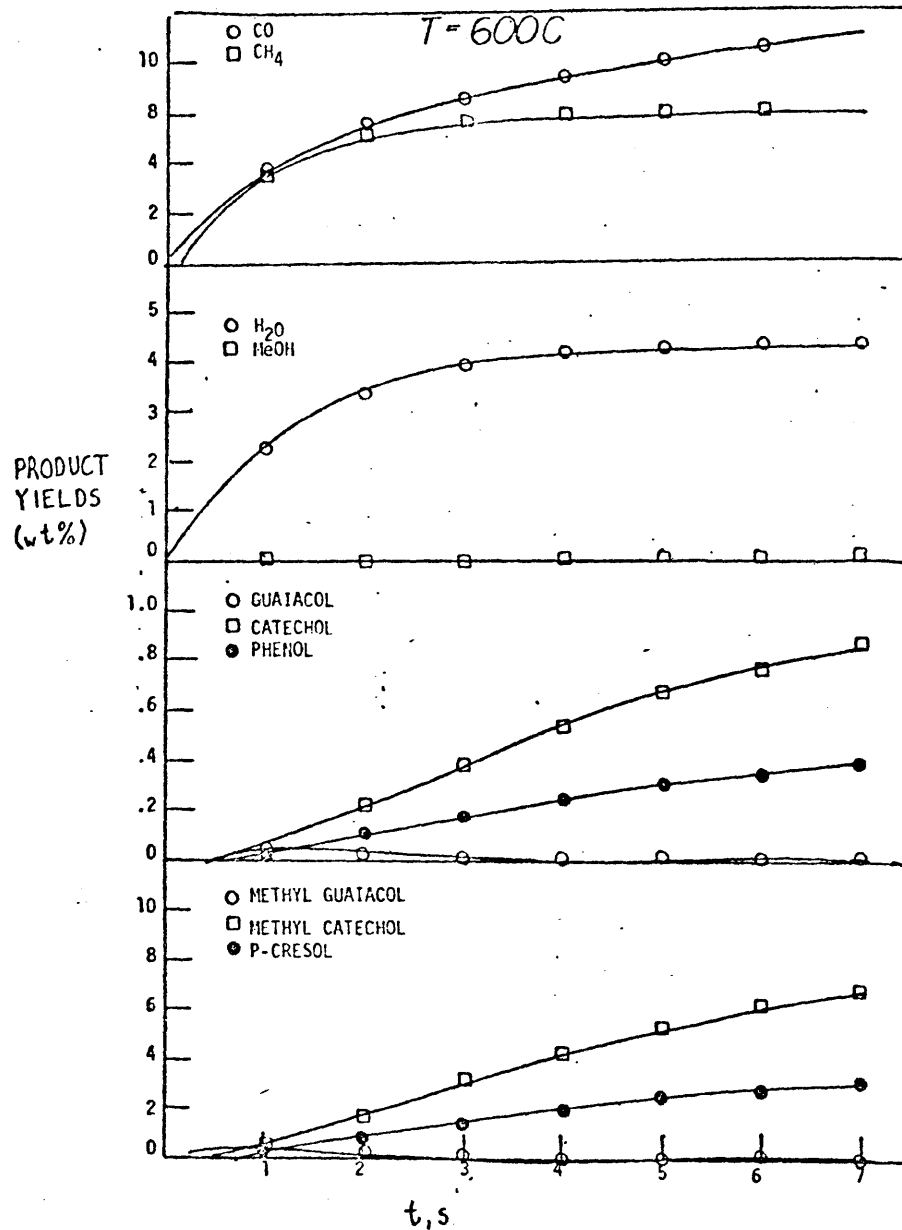


Figure 9.1c Model predictions at 600 C.

Simulation to 10^4 s at 300 and 400 C produced CO in yields of 0.037% and 3.5%, respectively. In both cases, these were less than the corresponding methane yield, yet initial rates of formation of CO at 400 C were faster than those for methane as seen at short times in Figure 9.1a. This early CO arises from the cinnamaldehyde side chains initially in lignin, which decarbonylate rather easily. At longer times, ether reversions generate further carbonyl and guaiacol units, the former through rapid saligenol dehydration. However, a large fraction of these carbonyls are of the acrolein type, which decarbonylate slower than cinnamaldehydes. Hence, CO release becomes slower than methane release as pyrolysis proceeds, the ratio CH_4/CO exceeding unity for modest conversions at 300 and 400 C. At the highest temperature of 600 C, however, CO again exceeds CH_4 as seen in Figure 9.1c, where the respective yields of CO and CH_4 are 9% and 6% at 7s. This occurs because CO producing pathways such as decarbonylation and demethoxylation are both more highly activated than the primary CH_4 producing pathway of guaiacyl demethanation. In short, the ratio CO/CH_4 is predicted to vary from greater than unity at low temperatures and low conversions, to less than one at low to modest temperatures and modest to long holding times, and back to greater than unity at high temperatures. This behavior originates in the dual sites for CO release and the relative kinetics of carbonyl, ether, and guaiacyl pyrolyses.

1.9.2 Liquid Products

The present version of the model accounts for only two components of the aqueous distillate, water and methanol. Simulation water formation occurs predominantly through saligenol-type unit dehydrations. Cinnamyl alcohol side chains provide less important precursors. Ultimate water yields were rather modest, amounting to 0.05%, 5.3%, 4.4%, and 4.4% at (300C, 10^4 s), (400C, 10^4 s), (500C, 10^2 s) and (600C, 7s), respectively.

Thus, the water yields predicted by the simulation are about 1/3 of the nominal $15\pm 5\%$ reported in experimental investigations. This discrepancy is significant, and merits later discussion.

An ultimate methanol yield of only about 0.1% is predicted by the simulation model. The single methanol forming pathway simulated is through degradation of cinnamyl alcohol side chain units. These units are rather rare in whole-lignin and the methanol forming pathway of this unit was itself relatively minor. Thus, the simulation model generally underpredicted methanol yields of the order 0.28-1.5% reported in the literature.

1.9.3 Phenolic Products

The simulation predicts most of the thirty phenols reported in previous experimental pyrolyses; it also predicts several phenolic products not hitherto reported in the literature. Overall, the product yields are within the band of yields reported in the literature. The simulation predictions will be discussed by phenol types.

Guaiacols

Guaiacols arise in lignin pyrolysis through degradations of both the 3-carbon side chain and etherified methoxyphenol substituents. Thus the products coniferaldehyde, guaiacylacrolein, eugenol, propylguaiacol, vinylguaiacol, ethylguaiacol, methylguaiacol, and guaiacol represent various stages of 3-carbon chain degradation. Of these, coniferaldehyde and guaiacylacrolein are the most primary products, degrading to vinylguaiacols, which, in turn, yield methylguaiacols, ethylguaiacol, and guaiacol upon further pyrolysis. These trends are reflected in the simulation predictions. At 400C and 100s the ratios (coniferaldehyde:vinylguaiacol:methylguaiacol:guaiacol) were (0.68: 0.13: 0.088: 0.011), whereas at 500s the proportions were (0.096:0.02:0.26:0.034) and at 10^4 s (0.000128:

0.000218:0.03:0.0039). By 10^4 s, the data reflect not only 3-carbon side chain degradation of the aldehyde, but also secondary pyrolysis of guaiacols to catechols. Each guaiacol product is both formed and degraded during pyrolysis, and therefore attains maximal proportions at some time.

Syringols (2,6-dimethoxyphenols)

With two exceptions, the reactions of syringol compounds directly mimic those of guaiacol compounds. The more important difference is the reaction path degeneracy inherent in syringols, on account of the multiple methoxyl substitution. The second exception involves lignification steric effects, which prevent the formation of biphenyl and phenylcoumaran links in aromatic units arising from sinapyl alcohol monomers. However, the consecutive and parallel nature of the reaction paths generating syringol products is substantially as described above for guaiacols.

Catechols

Rather substantial amounts of catechols are predicted by the simulation model, due to the relatively facile demethanation of guaiacol and substituted guaiacols. The catechols are clearly secondary products, favored at long holding times. These generalizations are reflected in the data. At 400 C and 100 s, the proportions (catechol:methylcatechol:vinylcatechol), in weight percent, were $(5 \times 10^{-4}:4 \times 10^{-4}:6 \times 10^{-3})$, whereas for pyrolysis to 10^4 s the yields were (0.2:1.6:0.012). At 500 C and 10 s holding time the ratios were (0.02:0.15:0.16), changing to (0.38:3.03:0.19) at 100 s. Finally at 600 C the proportions were (0.069:0.54:1.2) at 1 s and (0.86:6.8:1.2) at 7s. Thus, the yields of catechol and methylcatechol increased dramatically with increasing holding time at all temperatures. Note that this contrasts with the corresponding guaiacol yields, which reached maxima at short holding times and decreased monotonically there-

after with increasing time.

Phenols

Phenols arise from two sources, namely, aromatic units initially derived from incorporation of coumaryl alcohols during lignification, and from the demethoxylation reactions of guaiacol and syringol units. The statistical matching procedure demands that the phenol types be analogous to the guaiacols and syringols. Thus, simple phenol, cresol, ethylphenol, propylphenol, vinylphenol, allylphenol, coumaraldehyde, and hydroxyacrolein all arise as products. The simulated yields of phenol (PhOH) and para-cresols (pCR) were (PhOH,pCR) = ((0.00031, 0.0024), (0.067, 0.55), (0.16, 1.3), (0.39, 3.1)) at temperatures and times of ((300C,10⁴s), (400C,10⁴s), (500C,10²s), and (600C,7s). The absolute yields of phenols increased with increasing pyrolysis severity. the greater energy of activation for guaiacol demethoxylation relative to demethylation shifts the higher temperature selectivity toward phenols, even though absolute phenol yields were still lower than those of the corresponding catechols.

Carbonaceous Residue

As depicted by the present model, the carbonaceous residue is comprised of all aromatic units involved in interunit bonding. It should be characterized by higher concentrations of the refractory phenylether and diphenylmethane linkages than the initial lignin. Further, its methoxyl content should be markedly reduced relative to lignin due to demethanation and demethoxylation of guaiacyl and veratryl units. Finally, catechol and diquinone moieties should concentrate in the residue.

Carbonaceous residue formation can be interpreted in kinetic terms. Most kinetic analyses of lignin pyrolysis focus upon substrate weight loss, a reasonable operational definition of global lignin reactivity. In

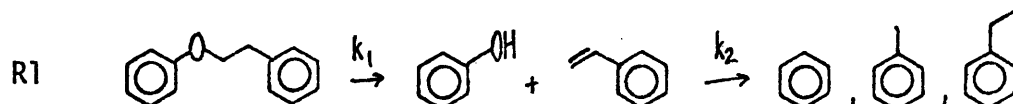
the present simulation, single ring aromatic units, light liquids, and gases can be designated as volatile, and multiple ring aromatics as non-volatile. If the latter group is considered to be 'unreacted lignin', the model then provides a measure of lignin 'conversion'. Figure 9.2 is a comparison between weight loss curves simulated in the present work and the experimental weight loss curves of Iatridis and Gavalas²⁶. The experimental and simulated weight loss curves align best at 500 C, with a slight simulation overprediction at 600 C and underprediction at 400 C; overall agreement is within about $\pm 10\%$ of the lignin.

1.10 Discussion

Two aspects of the present results merit discussion, namely the mechanisms of the experimental model compound pyrolyses and the application of the model pathways to simulate whole-lignin pyrolysis.

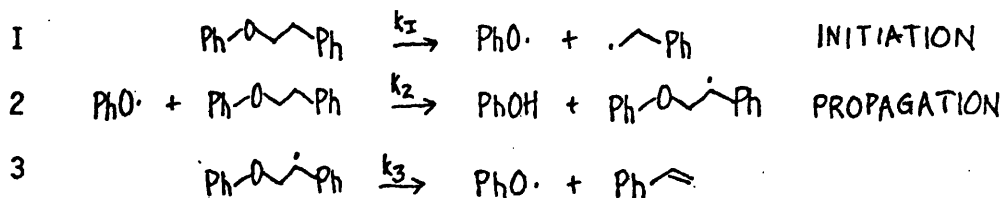
1.10.1 The Mechanism of Phenethyl Phenyl Ether (PPE) Pyrolysis

The relatively clean pyrolysis of PPE to phenol and styrene, earlier described in section 1.7.1, suggested an overall pathway of the type R1:



We attempt to interpret PPE pyrolysis in terms of both a free radical chain mechanism and a pericyclic retroene mechanism.

For neat PPE pyrolysis, a Rice-Herzfeld type of radical chain mechanism that yields the observed phenol and styrene products is:



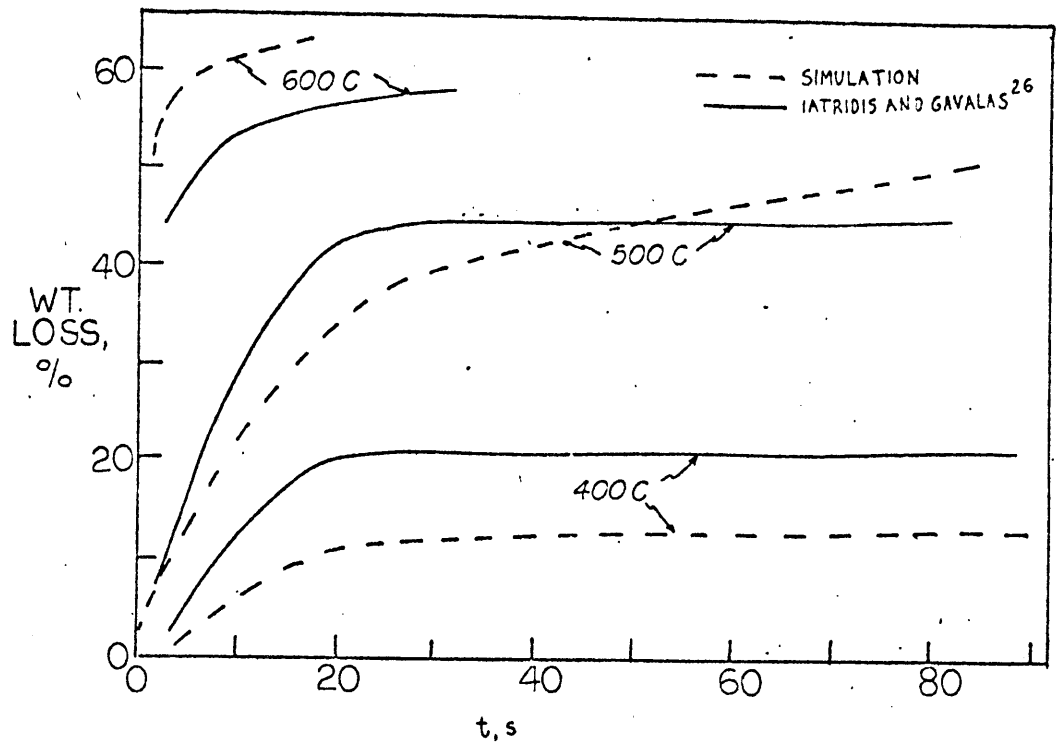
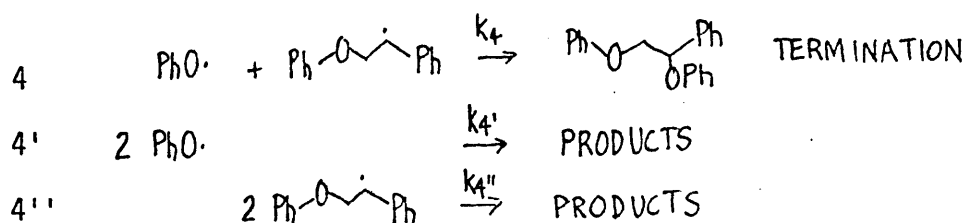


Figure 9.2 Comparison of simulation weight loss predictions with the experimental data of Iatridis and Gavalas²⁶



Invoking the steady state hypothesis for the radical species¹⁷⁵, and assuming long kinetic chain lengths, an overall PPE decomposition ex-

$$\begin{array}{l}
 5 \quad -dE/dt \approx k_2[\text{PhO}\cdot][E] = (2k_2k_3k_1/k_4)^{1/2} \cdot E \\
 5' \quad -dE/dt \approx k_2(2k_3/k_4')^{1/2} \cdot E^{3/2} \\
 5'' \quad -dE/dt \approx k_3(2k_1/k_4'')^{1/2} \cdot E^{1/2}
 \end{array}$$

pression can be derived. The kinetic expressions (5) are seen to depend upon the dominant termination step assumed, with steps (4), (4)', and (4)'' respectively yielding decomposition orders of 1, 3/2, and 1/2 in PPE.

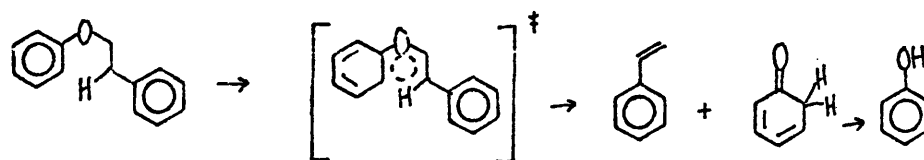
(Note $E \equiv \text{PPE}$) The experimentally observed order of 1 in PPE would thus imply cross-coupling (4) to be the major termination step. If this is so, then, from (5), the observed rate constant should equal $(2k_2k_3k_1/k_4)^{1/2}$. Estimated thermochemical parameters¹⁶⁹ for the elementary reactions 1, 2, 3, and 4 are $(\log_{10}A, E^*) = (17.0, 70.0), (9.0, 15.0), (13.0, 25.0)$ and $(9.0, 0.0)$, respectively. From them, the kinetic expression (5) provides first order Arrhenius parameters of (15,55). These parameters differ significantly from the present experimental Arrhenius parameters of (11.1,45.0), although at 400 C the estimated rate constant $\log_{10}k = -2.9$ is within half an order of magnitude of the experimental value of $\log_{10}k = -3.5$.

Further, a free radical chain such as (1)-(4) should be affected by a hydrogen-donor such as tetralin. The tetralin could cap the chain carrier radicals, hindering propagation. In the limit of infinite PPE

dilution in tetralin, the 'chain' would essentially be reduced to one of initiation only, i.e., the unimolecular fission of PPE to phenoxy and ethylbenzene radicals as the rate determining step. Such a unimolecular fission should proceed with an activation energy at least as great as the bond strength, which is of order $70 \pm 5 \text{ kcal/mol}$;¹⁶⁹ too, the accompanying transition state would be 'loose', resulting in $\log_{10} A > 13.5$. Experimentally, ether pyrolysis kinetics were unaffected by tetralin, and the observed Arrhenius parameters of $(\log_{10} A, E^*) = (11.1, 45.0)$ were strongly different from those predicted for unimolecular ether fission.

In summary, the long chain free radical mechanism represented a plausible possibility that did not accord with the present experimental observations.

A concerted pericyclic mechanism for the observed pathway R1 is:



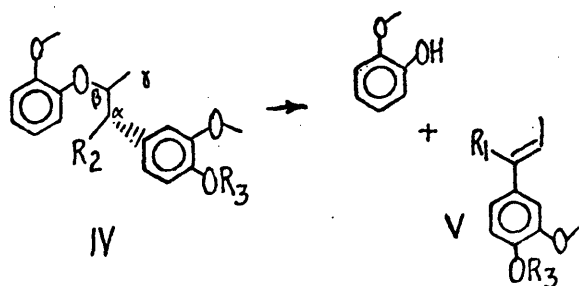
where a coiled form of the substrate PPE undergoes a retro-ene reversion; hydrogen tautomerism in the carbonyl intermediate fragment then regenerates the aromatic phenol. Such a PPE reversion to phenol and styrene should be unimolecular, exhibiting first order kinetics. The transition state of this state of this pericyclic pathway should be 'tight', i.e., ordered, making $\log_{10} A < 13.5$. Further, as for most pericyclic reactions¹⁷⁰, the decompositions should be relatively insensitive to solvent effects. Hence, tetralin should exert little overall effect on a PPE pyrolysis proceeding via a retro-ene mechanism. The experimental observations of the present work accord quite well with the postulated retro-ene mechanism.

By the principle of microscopic reversibility, the forward and re-

verse reactions must share a common transition state. If PPE reversion in fact occurs by the pericyclic mechanism postulated above, then the reverse reaction should occur with Arrhenius parameters characteristic of an ene cycloaddition. Estimation of thermochemical parameters for PPE¹⁶⁹, coupled with those for phenol and styrene, yields thermochemical parameters of $(\Delta H^\circ_R(\text{kcal/mol}), \Delta S^\circ_R(\text{cal/molK})) = (11.3, 33.8)$ for the reversion reaction. These may be combined with the experimentally determined forward activation parameters to yield the reverse cycloaddition parameters $(\log_{10} A(1/\text{mol s}), E^*(\text{kcal/mol})) = (5.9, 35.9)$. These reverse Arrhenius parameters agree well with those of typical bimolecular cycloaddition reactions^{167,171}.

In summary, a pericyclic retro-ene mechanism accords with the present experimental results for PPE pyrolysis.

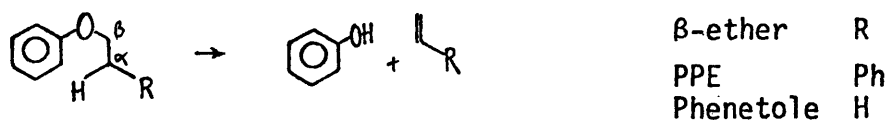
It is instructive to consider some previous β -ether pyrolyses^{75,76} in light of the present experimental and mechanistic findings for PPE. The investigation of Domburg⁷⁵ was previously described in section 1.4.2. DTA pyrolysis of three substituted β -ethers, I, II, and III (see page 19) gave product spectra consisting of guaiacol, methyl-, ethyl-, and propyl-guaiacols, cis- and trans-isoeugenol, traces of eugenol, vanillin, and acetovanillone; the latter two formed in much larger quantities from III than from I. The large predominance of guaiacol product, in their case, is completely analogous to the large yields of phenol obtained from PPE, inasmuch as their reactions may be viewed as:



Ether	R ₁	R ₂	R ₃
I	OH	H	H
II	OH	H	Me
III	O=	-	H
PPE	H	H	H

with appropriate modifications of structure V when emanating from ether III. Thus it is evident that guaiacol should predominate from pyrolysis of I-III, just as phenol was found from PPE. For pyrolysis of I and II, the co-product V can be visualized to suffer dehydration to yield the isoeugenols. For pyrolysis of III, co-product V can be envisioned as a facile precursor to vanillin and acetovanillone. Hence, formation of co-product V is rather analogous to the production of styrene from PPE. Further, the methyl-, ethyl-, and propylguaiacols can arise from V in much the same way that benzene, toluene, and ethylbenzene arose from secondary pyrolyses of styrene. Thus, the product spectra of Domburg can be almost completely accounted for by analogy to the present PPE results.

It should be further recalled that for Domburg's β -ethers, the temperatures for 50% weight loss were in the order I(280C)<II(300C)<<III(365C). The present work also provides a rationale for these observations. Thus, the pericyclic reversion mechanism is available to both I and II, but unavailable to III, for lack of an H substituent R₂ in III, which shifts in the retro-ene step. Thus, I and II may easily participate in a concerted retro-ene reaction of the type postulated for PPE, whereas an alternate, higher energy pathway is required for III. Possible higher energy pathways for III could involve direct scission of the β -carbon and oxygen atoms of structure IV, or a phenetole-type ether reversion involving the γ -carbon of structure IV. Phenetole is structurally similar to PPE, differing in phenyl substitution at the α carbon, as shown below:



Phenetole degradation has been studied by Benjamin, et al.⁷⁸, who report 5% substrate decomposition in tetralin after one hour at 400 C. Major

pyrolysis products included phenol, ethane, and ethylene. This conversion corresponds to an apparent first order rate constant of $\log_{10}k(s^{-1}) = -4.85$, which is over an order of magnitude lower than that for PPE at the same temperature. The α -phenyl substituent evidently enhances ether reversion considerably. The data of Savinykh⁷⁶, described earlier in section 1.4.2, also show that phenyl substitution enhances the pyrolysis of β -ethers.

1.10.2 Simulation of Lignin Pyrolysis

Discussion will begin with consideration of those literature citations which allow comparison with results of the present simulation. Overall yields of gas, liquid, phenolic and carbonaceous residue product fractions quoted in section 1.9 will be compared both with the literature yields and theoretical maximum limits. Individual product yields will also be discussed.

The matrix in Table 10.2.1 depicts items predicted by the present simulation which can be compared with previous literature. In the rows of this matrix, four major product fractions have been delineated in terms of overall and constituent component yields; the carbonaceous residue fraction subheading labeled 'kinetics' concerns the time dependency of overall lignin pyrolysis. The matrix has six columns, representing our model predictions and five sets of literature references. The latter include the collected reports of Table 4.1, the data of Iatridis and Gavalas²⁶, of Kirshbaum⁴¹, of Domburg³⁹, and the DTA/DTG data of Domburg and Sergeeva¹²⁹. In each matrix element, a plus indicates that information relevant to that row was reported, whereas an 'X' implies that it was not. The present simulation provides entries for each row save CO₂ yield. The overall gas fraction is the sum of CO and CH₄; these are by far the prevalent constituents of the lignin off-gas. The aqueous distillate was composed of water

Item	Model Prediction	Collected Authors Table 4.1	Iatridis and Gavalas ²⁶	Kirshbaum ⁴¹	Domburg ³⁹	Domburg and Sergeeva ¹²⁹
Gas Fraction						
Overall	+	+	+	+	X	X
CH ₄	+	+	+	X	X	X
CO	+	+	+	X	X	X
CO ₂	X	+	+	X	X	X
Aqueous Fraction						
Overall	+	+	X	X	X	X
H ₂ O	+	+	X	X	X	X
MeOH	+	+	+	X	X	X
Phenolic Fraction						
Overall	+	+	+	+	+	X
Individual Phenols	+	X	+	+	+	X
Carbonaceous Residue						
Overall	+	+	+	+	X	X
Kinetics	+	X	+	X	+	+

+ relevant information provided

X no relevant comparison possible

Table 10.2.1

Literature references relevant for comparison with simulation predictions

and methanol only; acetone, acetic acid and other minor liquid products were not included in the simulation. The phenolic fraction was the molar sum of all single ring phenols; this overall yield should correspond best to the overall tar yield reported in pyrolysis experiments. Finally, the carbonaceous residue fraction is composed of all multiple ring aromatic units. The investigations collected in Table 4.1 provide detailed accounts of gas and aqueous distillate yields, and overall tar and char yields. Because detailed temperature-time information is lacking for many of these investigations, entries in this column are best considered the asymptotic, 'ultimate', yields of destructive distillations. The data of Iatridis and Gavallas²⁶ were obtained in a reactor designed to emphasize primary reactions, providing detailed temperature-time information and entries for all save overall aqueous distillate yields and water yields. Kirshbaum⁴¹ provided overall gas, phenolics, and carbonaceous residue yields; detailed phenolic product spectra were provided also. Detailed descriptions of phenolic product spectra were also given by Domburg³⁹. Finally, Domburg and Sergeeva¹²⁹ provide DTA/DTG weight loss information for lignin decomposition.

A numerical summary of the product yields predicted by the simulation and reported in the literature is presented as Table 10.2.2, a matrix completely analogous to that in Table 10.2.1. The discussion to follow considers each row of Table 10.2.2; note that all yields are in weight percent of original lignin substrate.

Gas Fraction

The simulated overall gas fraction rose steadily with increasing time and temperature and achieved a value of about 15% at 600 C. This compares favorably with the data of Table 4.1, where gas yields ranged

Item	Model Prediction	Collected Authors: Table 4.1	LITERATURE		
			Iatridis and Gavalas ²⁶	Kirshbaum ⁴¹	Donburg ³⁹ Donburg and Sergeeva ¹²⁹
Gas Fraction					
Overall yields	15% @ 600C	10-20%, 15% mean	23% max including CO ₂	5% @ 250C, 16% @ 600C gases and losses	X
CH ₄	6% @ 600C	7% based on mean overall yield of 15%	4.8% @ 650C	X	X
CO	9% @ 600C	7% based on overall mean of 15%	9.2% @ 650C	X	X
CO ₂	X not included in simulation	1.5%	near 6%, all temperatures	X	X
Aqueous Fraction					
Overall	6% maximum	overall mean 15%	X	X	X
H ₂ O	6% maximum	12-15%	X	X	X
MeOH	0.1% maximum	0.2-1.0%	3% @ 650C	X	X
Phenolic Fraction					
Overall	Sum of single ring phenols as function of time: 7-80%, include complex phenols	3-30%	0.3-3.0%, 400-650C	3.3-14.5% @ 475C	0.2% @ 250C, 14% @ 500C
Individual Phenols	Detailed yields of individual phenols as a function of time and temperature	X	only guaiacols and phenols	detailed yields of 20+ different phenols	detailed yields of 20+ different phenols
Carbonaceous Residue					
Overall	Ultimate residue yield from 0.914 @ 300C to 0.335 @ 600C	40-60% yield of char	weight loss of 53% @ 600C	char yield of 91% @ 250C, 26% @ 600C	X
Kinetics					
	multiple ring aromatics as function of time, ultimate yields as function of temperature	X	weight loss for 400-600C as in function of time	X	DTA/DTG experiments yield E 26-30 kcal/mol DTA/DTG experiments yield E 18-38 kcal/mol

Table 10.2.2 : Quantitative simulation literature comparison grid.

from about 10-20%. Iatridis and Gavalas report an overall yield as high as 23% at 650 C, but this included 7.2% CO₂. As discussed below, this rather high CO₂ content may be due to their use of a Kraft lignin. Omitting CO₂, their overall gas yield is 16%, in good agreement both with the simulation and earlier literature. Additionally, Kirshbaum reports total gas (and losses) yield of ~5% at 250 C and ~18% at 600 C.

Theoretically, the maximum overall gas yield should be a function of temperature. At low temperatures, methoxyphenols prevalently release methane gas; assuming an ideal release of one mol of methane per methoxy unit, a maximum methane yield of ~9% arises. Further, assuming a release of one mol of CO per side chain, a low temperature CO maximum of ~15% arises. At low temperatures, a maximum total gas yield of ~24% by weight of lignin is thus calculated, comprising CH₄ and CO in the ratio 2:3. With increasing temperature, methoxyphenol gas release selectivity shifts toward CO evolution, and thus in the limit of high temperatures, two mols of CO will be produced from each aromatic unit in lignin; a corresponding overall gas yield of ~30% thus arises, composed entirely of CO.



The simulated time-dependency of methane yield at several temperatures was earlier detailed in Figures 9.1a-c. Based on 15% average total gas yields from DTA and destructive distillation of lignin, Table 4.1 provides methane yields of 7.1%. This agrees quite well with our simulated yield of 6.2% at 400 C and 10⁴s. Iatridis and Gavalas reported methane yields of 2.21% at 500 C and 60 s, and 1.3% at 600 C and 10 s. The simulation predicted methane yields of 5.1% at 500 C and 60 s and 6.1% at 600 C and 7s. Thus our simulation overpredicted methane yield as compared to the data of Iatridis and Gavalas. This discrepancy likely arises be-

cause, on the one hand, the pyrolyser of Iatridis and Gavalas was designed to emphasize primary reactions, such that primary products could leave the 'reaction zone' without secondary pyrolysis. On the other hand, our simulation models a batch reactor, where primary products, such as guaiacols, were subjected to extensive secondary pyrolyses, yielding more catechols and methane. Also, Kraft lignins, used in this experiment, are known to have a lower methoxyl content than the simulated spruce lignin substrate; this contributes to the discrepancy between experimental and simulated methane yields.

CO

The simulation predicted CO evolution in yields of 0.037%, 3.5%, 4.4%, and 9% at (300C,10⁴s), (400C,10⁴s), (500C,60s), and (600C,7s), respectively. These yields are in substantial agreement with the literature citations noted in Table 4.1. As in the case of methane, simulated CO yields generally exceeded those reported by Iatridis and Gavalas. These workers report 1.2%, 2.1%, 2.7%, and 9.2% at (400C,120s), (500C,60s), (600C,10s), and (650C,120s), respectively, whereas simulated yields were 0.22%, 4.4%, and 9% at (400C,100s), (500C,60s), and (600C,7s), respectively. Interestingly, the experimental CO/CH₄ ratio varied from about 2.3 at 400 C to 0.88 at 500 C and 1.8 at 600 C, which closely accords with the behavior of this ratio in our simulation. This was earlier interpreted in terms of dual carbonyl and methoxyphenol sites for CO release from lignin.

Aqueous Distillate

Based on the sum of water and methanol yields, the simulation predicted an overall distillate yield of about 6%, rather lower than the yields of ~15% reported by the literature references in Table 4.1. Water is by far the most prevalent component of the overall aqueous distillate,

with methanol (0.3 to 2%), acetic acid (0.1 to 1.0%), and acetone (0.1 to 1.0%) as minor components. Theoretically, assuming the release of one H_2O mol per 3-carbon side chain, a maximum water yield of $\sim 10\%$ is calculated. However, aqueous distillate yields higher than 10% are reported in the literature (cf Table 4.1); these are likely due to physically associated water either extant in the plant lignin or introduced during lignin isolation. Another possible source of water is the carbohydrate impurity invariably present in lignin preparations.

H_2O

Our simulation predicted ultimate water yields of 6%. Absolute water yields have not often been experimentally measured. However, taking account of the minor components methanol, acetone, and acetic acid in the aqueous distillate, an average water yield of 12-13% can be estimated from Table 4.1. The experimental yield is significantly higher than predicted in our simulation, which suggests that the latter requires further sources for water formation in the lignin; kinetic limitations are precluded by the rapidity of saligenol dehydration. Physically adsorbed water and saturated hydroxyl groups are possible precursors for further water yields. The former has already been discussed. As for the latter, formal hydroxyl cleavage could conceivably produce two water mols from guaiacyl-glycerol- β -ethers, and thus increase net water formation from lignin to as much as 13%.

MeOH

An ultimate methanol yield of 0.1% is predicted by the simulation. This is substantially less than the yields of 0.28 to 1.5% reported in Table 4.1 and the yield of 2% obtained by Iatridis and Gavalas. The reasons for our smaller methanol predictions are not yet clear, and could

involve both kinetic limitations and alternative lignin pathways. With regard to the former, the simulated pathway to methanol was through degradation of cinnamyl alcohol side chains. This reaction was subject to considerable experimental uncertainty and a greater rate constant would increase the predicted selectivity to methanol. Alternative methanol forming pathways, not delineated in the present model compound pyrolyses, may well operate in whole-lignin pyrolysis. This is an area for further experimental investigation. However the experimental results obtained here and reported in the literature^{91,96} do indicate that methanol formation from methoxyphenols, the obvious moieties for demethoxylation, is not significant.

Phenolic Fraction

The predicted overall yield of single ring phenols ranged from 7-80%. These represent lignin aromatic units that were transformed into single ring aromatics during simulated pyrolysis. Included in this single ring phenol yield are substantial amounts of complex phenols, such as coniferaldehyde and guaiacyl vinyl ketone (or guaiacyl acrolein), which are not often reported with single ring phenols in experimental pyrolyses. Experimental overall phenolic fraction yields were 3 to 30% for Kirshbaum, and 0.2 to 14% for Domburg. These were lower than the simulation for two likely reasons. First, many complex phenols in the tar fraction were not experimentally identified. It is cogent to note that tar yields in excess of 50% have been reported⁷¹. Second, the simulation suppressed bimolecular condensation and polymerization reactions which would have lowered the yield of single ring phenols.

Individual Phenols

As noted earlier, the present simulation predicts most of the

thirty-odd phenols detected in the previous experimental pyrolyses. The accuracy of these individual phenol yield simulations is uncertain, on account of the wide range of lignin types, isolation methods, and reactor configurations employed in experimental studies. These provide a rather generous band for comparison with model predictions. In most cases the predicted and experimental yield data agreed to within a half-order of magnitude. Larger deviations, such as those related to guaiacol, catechol and syringol, could be reasonably explained by inherent differences between simulated and experimental conditions. In particular, it is noteworthy that deviations between the present simulation and experiment were no greater than deviations between individual experiments.

Carbonaceous Residue

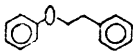
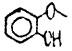
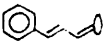
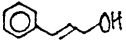
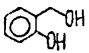
The simulated carbonaceous residue yields of 91% at 300 C and 10^4 s and 40% at 600 C and 7s compare favorably with the literature. In Table 4.1, ultimate tar yields from destructive distillation were 40 to 60% of lignin. Iatridis and Gavalas report weight losses of 20% and 53% at 400 and 600 C, respectively, corresponding to char yields of 80% and 47%. Kirshbaum reports a char yield of 91% at 250 C and only 26% at 600 C. In short, the present operational definition of residue as multiple ring aromatics provides simulated carbonaceous residue yields that are in good accord with the experimental literature.

Weight Loss Kinetics

The residue-forming kinetics implied by the time variation of the simulated yield of multiple ring aromatic units have earlier been compared in Figure 9.2 with the data of Iatridis and Gavalas. The simulated weight loss curves accorded well with the experimental weight loss curves, with modest deviations at the lowest and highest temperatures. Furthermore,

these deviations can reasonably be attributed to differences between the respective lignin substrates. Iatridis and Gavalas used a Douglas fir precipitated Kraft lignin, whereas the present simulation was based on Freudenberg's unperturbed "protolignin". Kraft pulping can alter the chemical nature of lignin substantially. It results in increased internal condensations, with the original reactive α - and β -ether linkages transformed into less reactive diphenyl-methane, ethane, and ethylene linkages; it also introduces carboxylic acid units into the lignin macromolecule. The low temperature reactivity of a Kraft lignin might be expected to be greater than its protolignin counterpart because of facile CO_2 evolution from the carboxylic acid units. At higher temperatures and conversions, however, the reactivity of a Kraft lignin may well be lower than that of the protolignin since relatively refractory diphenylmethane, ethane and ethylene units have replaced the original reactive α - and β -ethers. In the light of these assertions it is interesting that Iatridis and Gavalas report CO_2 yields of 5.9% at 400 C and 120s, and 4.1% at 600c and 10s. These suggest a constant number of easily decarboxylated acid sites in their substrate. Further, these authors' reported weight loss of 20% at 400 C and 120s exceeds our simulated weight loss of 13% by an amount substantially equal to their CO_2 yield. At 600 C and 10s the experimental weight loss corrected for CO_2 is ~50%, somewhat lower than our simulated value of 60% on account of the reduced reactivity of their Kraft lignin.

1.11 Summary and Conclusions

1. Theoretical analysis of Freudenberg's classical spruce lignin structure permitted the selection of model chemical compounds that would mimic the reactivity of lignin during its thermal degradation. Some of the model compounds chosen, and their attributes relevant to lignoid moieties, were: Phenethylphenylether (PPE) , for the prevalent β -ether linkage: Guaiacol, , for the aromatic methoxyphenol unit: Cinnamaldehyde  and Cinnamyl alcohol , for the propanoid side chain and saligenol, , for the hydroxy enol that might form in lignin following β -ether reversion.

2. Experimental pyrolyses of each of 20 model compounds were undertaken to determine hitherto unknown reaction pathways, kinetics, and activation parameters. The products from these model pyrolyses were closely analogous to those observed in actual lignin thermolysis, including methane (from guaiacol), carbon monoxide (from cinnamaldehyde), water (from saligenol), methanol (from cinnamyl alcohol), and phenol (from PPE).

3. Mechanistic interpretations of pyrolysis pathways were possible in at least five instances. For example, PPE reverted stoichiometrically to phenol plus styrene as primary products; at 400 C the reaction was first order in PPE over a twentyfold range of initial concentrations and unaffected by tetralin dilution; at temperatures from 300 to 500 C, the rate constant followed an Arrhenius relationship, with $(\log_{10} A(s^{-1}), E^*$ (kcal/mol)) = (11.0 \pm 0.9, 45.0 \pm 2.7). These experimental data were well rationalized by a concerted, pericyclic retro-ene reaction mechanism. Similarly, methane elimination from guaiacol, $(\log_{10} A, E^*) = (10.9, 43.7)$, and water elimination from saligenol, (13.4, 33.4), could both be well interpreted as concerted, pericyclic group transfers.

4. It appears that the molecular topology of lignin is well suited to the occurrence of concerted pericyclic reactions, which have not hitherto been mentioned in the lignin pyrolysis literature. Likely examples of pericyclic pathways found in the present experiments included:

- (i) Retroene reversion of Phenethylphenylether.
- (ii) Group transfer demethanation of guaiacols and group transfer dehydration of saligenol.
- (iii) Sigmatropic methyl shifts in anisole and veratrole to o-cresol, the latter with subsequent retroene release of CO and H₂. An analogous hydrogen shift for guaiacol demethoxylation is likely.
- (iv) Cheletropic extrusion of CO from benzaldehyde, vanillin, and cinnamaldehyde, with calculated reverse carbonylation Arrhenius parameters consistent with those of concerted cycloadditions.
- (v) Diels-Alder cycloaddition reactions for cinnamaldehyde and cinnamyl alcohol side chain units, of the type reported in the literature for styrene and acrolein.

5. Mathematical simulation of whole-lignin pyrolyses, at 300 to 600 C with holding times of 1 to 10⁴ s, was achieved by combining a statistical interpretation of lignin structure with experimental results of the present model compound pyrolyses. The outcome of these simulations, expressed in terms of product fractions as a percent of initial lignin, was:

- (i) Gas Fraction: Simulated overall gas, methane, and CO yields accorded with previous experimental lignin pyrolyses; respective ultimate yields typically 15%, 6%, and 9% were in quantitative agreement with the literature of Table 4.1. The simulated variation of (CH₄/CO) ratio with time and temperature further agreed with that recently reported by Iatridis and Gavalas²⁶.

(ii) Aqueous Fraction: Simulated water yields were typically about half the reported experimental yields of 12%. Simulated methanol yields were half an order of magnitude lower than the literature yields of 0.3-1.5 %.

(iii) Phenolic Fraction: Simulated overall phenolic yields were generally higher than the literature yields by a factor of two. The simulation accounted for more than thirty individual phenols reported in the literature. Simulated yields of simple guaiacols, catechols, syringols, and phenols, each nominally 2%, were within the band of values reported in the literature.

(iv) Carbonaceous Residue: Simulated curves of weight loss versus time at 400, 500, and 600 C were nearly coincident with the experimental curves due to Iatridis and Gavalas²⁶ for pyrolysis of a Kraft lignin. Also, the modest disagreements between these curves, at both low and high temperatures, were traced to structural differences between the respective lignin substrates.

1.12.0 References

2. Energy Alternatives: A Comparative Analysis, Report prepared by Science and Public Policy Program at the University of Oklahoma, Stock #041-001-00025-4, U. S. Gov't Printing Office, Wash., D.C. (1975)
4. Freudenberg, K.; Neish, A. C., Constitution and Biosynthesis of Lignin, Springer-Verlag, New York (1968)
5. Harkin, J. M., in Battersby and Taylor, Oxidative Coupling of Phenols, Marcel-Dekker (1967)
19. Wenzyl ; H.F.J., The Chemical Technology of Wood, Academic Press, New York (1970)
23. Heuser, E. 1 Skioldebrand, C., Z. angew. Chem., I, 32, 41 (1919)
- 24a. Klason, P; Haindenstam, G.v.; Norlin, E., Z. angew Chem., 22, 1205 (1909)
- b. Klason, P; Haindenstam, G.v.; Norlin, E., Z. angew Chem, 23, 1522 (1910)
- c. Klason, P; Haindenstam, G.v.; Norlin, E., ArkivKemi. Mineral, Geol., 3 no. 1 (1907)
- d. Klason, P.; Haindenstam, G.v.; Norlin, E., ArkivKemi. Mineral. Geol., 3 no. 10 (1908)
25. Gladkova, N. Ya.; Sokolova, N. A.,; Levin, E. D., Khim. Ispol'z Lignina, 434 (1974)
26. Iatridis, B. and Gavalas, G. R., Ind. Eng. Chem. Prod. Res. Dev., 18(2), 127 (1979)
27. Mikulich, S. M.; Mikulich, A. S., Svoistva Strukt. Gazov, Zhidk, Tverd. Tel, 52-65 (1975)
29. Goheen and Henderson in Allan, G. G.; Matilla, T., op. cit. 30
30. Allan, G. G.; Mattila, T., in Sarkanen, K. V. and Ludwig, C. H., Lignins Occurrence, Formation, Structure and Reactions, Wiley Interscience, New York (1971)
31. Szelenyi, G., Gomory, A., Brennstoff-Chem. 9, 72 (1928)
32. Heuser, E.; Brotz, A., Papier-Fabrik., 23, Fest-und Ausland-Heft, 69 (1925)
34. Phillips, M., J. Am. Chem. Soc., 51, 2420 (1929)

35. Bridger, G. L., *Ind. Eng. Chem.*, 30, 1174 (1938)
38. Domburg, G. E.; et al., *Khim, Drev.* no. 5, 64 (1976)
39. Domburg, E. E., et al. *Thermal Analysis of Lignin in Thermal Analysis Vol. 3 Proc. 3rd ICTA Davos (1971) pp 327-40.*
Burkhaeuser, Basel 1972
40. Panasyuk, L. V.; Travleeva, L. V.; Panasyuk, V. G., *Khim. Drev.* 1:301 (1968)
41. Kirshbaum, I. Z.; Domburg, G. E., Sergeeva, V. N. *Khim. Drev.* no. 4, 96 (1976)
42. Kirshbaum, I. Z.; Domburg, G. E., *Izv. Akad. Nauk Latv.* 55R no. 2, 43 (1970)
43. Vorher, W.; Schweers, W. H. M., *G. Appl. Polymer Sci. (Appl. Polymer Symp)* no. 28, 277 (1975)
44. Faix, O.; Schweers, W.; *Holzforschung* 29, no. 6, 224 (1975)
48. Gillet, A; Urlings, J., *Chim & Ind. (Paris)*, 68, 55 (1952)
49. Panasyuk, V. G.; Maksimenko, N. S., *Gidroliz. i Lesokhim. Prom.* 11, no. 1, 16-17 (1958)
52. Prosinski, S.; Czechowski, Z.; Kielczewski, M., *Koks. Smola. Gaz.* 15, no. 11, 322 (1970)
53. Hagglund, E., *Arkiv. for Kemi, Min. och Geol.*, 7, 1 (1918)
54. Phillips, M.; Goss, M. J., *Ind. Eng. Chem.*, 24, 1436 (1932)
55. Fisher, F., Schrader, H., *Ges. Abhandl. Kenntnis Kohle*, 5, 106 (1922)
56. Tropsch, H., *Ges. Abhandl. Kenntnis Kohle*, 6, 293 (1921)
57. Picteti, A.; Gaulis, M., *Helv. Chim. Acta*, 6, 627 (1923)
58. Fletcher, T. L.; Harris, E. E., *Tappi*, 35, 536 (1952)
59. Kurth, E. E.; Ervin, H. O.; Kroll, R. L., *J. Am. Chem. Soc.*, 58, 571 (1955)
- 60a. Shimaboto, T., et. al., *J. Japan Forestry Soc.*, 32, 43, 47, 75 (1950)
 - b. Shimaboto, T.; Minami, K.; Kadama, T., *J. Japan Forestry Soc.*, 34, 77 (1952)
 - c. Shimaboto, T.; Minami, K.; Sakai, H., *J. Japan Forestry Soc.*, 33, 12 (1951)

61. Panasyuk, V. G., Zhurn. prikl. Khim., 34, 1409, 1605 (1958)
62. Fletcher, T. L.; Harris, E. E., J. Am. Chem. Soc., 69, 3144 (1947)
63. Morozov, E. F., Gidroliz, Lesokhim. Prom. 23, no. 7, 15 (1970)
65. Gracheve, E. V.; Levin, E. D. Izv. Vuz. Lesnoi. Zh. 19, no. 2, 108 (1976)
71. Domburg, G. E.; Kirshbaums, I.; Sergeeva, V. N., Khim. Drev., 7, 51 (1971)
75. Domburg, G. E., Thermal Analysis, 2 Proc. 4th ICTA, Budapest (1974)
76. Savinykh, V. I., et al., Khim. Drev., 5, 100 (1975)
77. Kislitsyn, A. N., et al., Khim Drev., 9, 131 (1971)
78. Benjamin, B. M. et al., Fuel, 57, 270 (1978)
79. Kayima, Y., et al., ACS Div. of Full Chem. preprints, 24 (2), 116 (1979)
80. Miller, R. E. and Stein, S. E., ACS Div. of Full Chem. preprints, 24 (3), 271 (1979)
81. Savinykh, V. I., et al., Khim. Drev., 3, 91 (1976)
82. Ingold, K. V. and Lossing, F. P., Can. J. of Chem., 31, 30-41 (1953)
91. Shaposhnikov, Uy. K. and Kosyukova, L. V., Khim. Pererabotka Drev., Ref. Inform., no. 3, 6-9 (1965)
92. Kravchenko, M. I.; Kiprianov, A. I.; Korotov, S. Ya; Nauch. Tr. Leningrad Lesotekh. Akad., 135 (2), 60-4 (1970)
93. Kiprianov, A. I. and Kravchenko, M. I., Izv. Vyssh. Ucheb. Zaved., Les Zh. 15 (5), p 121-5 (1972)
94. Kislitsyn, A. N. ; Rodionova, Z. M.; Savinykh, V. I.; Ill'ina, E.I.; Abakhumov, G. A., Sb. Tr., T sent. Nauch - Issled. Prockt. Inst. Lesokhim. Prom., no. 22, p 4-16 (1971)
95. Friedlin, L. Kh; Balandin, A. A.; Nazarova, N. M.; Izvest. Akad. Nauk S.S.S.R., Otdel Khim. Nauk, no. 1, 102-9 (1949)
96. Obolentsev, R. D., J. Gen. Chem. (U.S.S.R.) 16, 1959-70 (1946)
97. Kislitsyn, A. N., et al., Zh. Prikl. Khim (Leningrad) 45 (2), 384 (1972)

98. Smith, R. E. and Hinshelwood, C. N., Proc. Roy. Soc., (London) A, 175, 131-142 (1940)
99. Domburg, G. E.; Sergeeva, V. N.; Zheibe, G. A.; Khim. Drev., 7 59 (1971)
100. Kislitsyn, A. N.; et.al., Khim. Drev., 9, 125 (1971)
101. Sprengling, G. R., J. Am. Chem. Soc., 74, 2937 (1952)
129. Domburg, G. E.; Sergeeva, V. N., J. Thermal, Anal. 1, 53 (1969)
164. Mademov, S. and D. N. Khydyrov, Zhurnal Obshchei Khimii, 32 (5), 1427 (1962)
167. Frey, H. M., and Walsh, R., Chem. Rev., 69 103 (1969)
169. Benson, S. W., Thermochemical Kinetics, Wiley, New York (1968)
Benson, S. W., et al., Chem. Rev., 69 279 (1969)
170. Woodward, R. B. and Hoffmann, R., The Conservation of Orbital Symmetry, Verlag Chemie, Academic Press, Germany (1971)
171. Mock, W. L. in Pericyclic Reactions Volume II, A. P. Marchand and R. E. Lehr, Editors, Academic Press, New York (1977)
175. Froment, G. F. and K. B. Bischoff, Chemical Reactor Analysis and Design, Wiley, (1979)
178. Dulong, L., Markromol. Chem., 76, 119 (1964)
179. Bjorkman, A, Nature, 174, 1057 (1954); Svensk Papperstid, 59, 477 (1956)
180. Yu, K. C., S. B. Thesis, MIT, June, 1980

Work reported in this document was sponsored by the Department of Energy. This report was prepared as an account of work sponsored by the United States Government. Neither the United States nor the United States Department of Energy, nor any of their employees, makes any warranty, express or implied, or assumes any legal liability or responsibility for the accuracy, completeness, or usefulness of any information, apparatus, product or process disclosed or represents that its use would not infringe privately owned rights.